Chemical composition, main sources and temporal variability of PM$_1$ aerosols in southern African grassland

P. Tiitta[1,2,6], V. Vakkari[3,5], P. Croteau[4], J. P. Beukes[2], P. G. van Zyl[2], M. Josipovic[2], A. D. Venter[2], K. Jaars[2], J. J. Pienaar[2], N. L. Ng[7], M. R. Canagaratna[4], J. T. Jayne[4], V.-M. Kerminen[3], H. Kokkola[5], M. Kulmala[3], A. Laaksonen[5,6], D. R. Worsnop[3,4,6], and L. Laakso[2,5]

[1]Department of Environmental Science, Univ. of Eastern Finland, P.O. Box 1627, 70211 Kuopio, Finland
[2]School of Physical and Chemical Sciences, North-West University, Potchefstroom 2520, South Africa
[3]Department of Physics, Univ. of Helsinki, P.O. Box 64, 00014 Helsinki, Finland
[4]Aerodyne Research, Inc., Billerica, MA 08121, USA
[5]Finnish Meteorological Institute, Erik Palménin aukio 1, 00101 Helsinki, Finland
[6]Department of Applied Physics, Univ. of Eastern Finland, P.O. Box 1627, 70211 Kuopio, Finland
[7]School of Chemical and Biomolecular Engineering and School of Earth and Atmospheric Sciences, Georgia Institute of Technology, Atlanta, GA 30332-0100, USA

Correspondence to: P. Tiitta (petri.tiitta@uef.fi)

Abstract. Southern Africa is a significant source region of atmospheric pollution, yet long-term data on pollutant concentrations and properties from this region are rather limited. A recently established atmospheric measurement station in South Africa, Welgegund, is strategically situated to capture regional background concentrations, as well as emissions from the major source regions in the interior of South Africa. We measured non-refractive submicron aerosols (NR-PM$_1$) and black carbon over a one year period in Welgegund, and investigated the seasonal and diurnal patterns of aerosol concentration levels, chemical composition, acidity and oxidation level. Based on air mass back trajectories, four distinct source regions were determined for NR-PM$_1$. Supporting data utilised in our analysis included particle number size distributions, aerosol absorption, trace gas concentrations, meteorological variables and the flux of carbon dioxide.

The dominant submicron aerosol constituent during the dry season was organic aerosol, reflecting high contribution from savannah fires and other combustion sources. Organic aerosol concentrations were lower during the wet season, presumably due to wet deposition as well as reduced emissions from combustion sources. Sulfate concentrations were usually high and exceeded organic aerosol concentrations when air-masses were transported over regions contain-

ing major point sources. Sulfate and nitrate concentrations peaked when air masses passed over the industrial Highveld (iHV) area. In contrast, concentrations were much lower when air masses passed over the cleaner background (BG) areas. Air masses associated with the anti-cyclonic recirculation (ACBIC) source region contained largely aged OA.

Positive Matrix Factorization (PMF) analysis of aerosol mass spectra was used to characterise the organic aerosol (OA) properties. The factors identified were oxidized organic aerosols (OOA) and biomass burning organic aerosols (BBOA) in the dry season and low-volatile (LV-OOA) and semi-volatile (SV-OOA) organic aerosols in the wet season. The results highlight the importance of primary BBOA in the dry season, which represented 33 % of the total OA. Aerosol acidity and its potential impact on the evolution of OOA are also discussed.

1 Introduction

Africa is one of the least studied and most sensitive continents with regard to climate change and air pollution (Boko et al., 2007; Forster et al., 2007). Therefore, long-term atmospheric observations are required to study various effects

and drivers. South Africa has one of the largest economies in Africa and is currently the only industrialised regional energy producer on the continent. South Africa has had sustained economic growth for a number of years, resulting in increasing fossil fuel consumption and demand for electricity. Most of the electricity in southern Africa is produced by coal-fired power stations. A substantial fraction of petrol is also distilled from coal as well as obtained from natural gas. Additionally South Africa has a large mining and associated metallurgical industry (e.g., Beukes et al., 2010). Domestic combustion for space heating and cooking is also widely practiced, especially in informal settlements that occur around most towns/cities (e.g., Venter et al., 2012; Vakkari et al., 2013). All of the afore-mentioned has led to increased environmental concerns with atmospheric pollution being a major problem.

Even though new industrial operations in South Africa are being equipped with cleaner technology and the scrubbing facilities of old operations are being improved, emissions of sulphur dioxide (SO_2), nitrogen oxides (NO_x), black carbon (BC) and carbon dioxide (CO_2) are estimated to increase. These emissions, combined with potential increase in biomass burning due to global warming the associated dryer climate in certain parts of southern Africa, can significantly influence the regional and global climate (Boko et al., 2007).

Climate change may also enhance migration to the already densely populated urban areas and potentially increase environmental problems. As the population in cities in developing countries (such as those in southern Africa) increases, effects of air pollution on human health and the ecosystems will become more important.

Currently, air pollution monitoring studies in South Africa are focused mainly on legislatively required measurements of particulate matter (PM$_{10}$ – particles with diameter less than 10 μm) and gaseous pollutants such as SO_2, NO_x and ozone (O_3), as well as benzene and lead (Martins et al., 2007; Josipovic et al., 2010; Lourens et al., 2011). Recently, Venter et al. (2012) conducted an air quality assessment at a site situated in an industrialised region with significant mining and metallurgical activities. A limited number of these types of studies have been published in the peer reviewed literature. Very few comprehensively equipped long term operating atmospheric measurement stations exist in South Africa. Most stations are equipped with limited instrumentation, or data from comprehensive equipment sets are operated only for short campaigns. One exception is the Cape Point Global Atmospheric Watch (GAW) station (Brunke et al., 2010) in the marine-boundary layer where long-term trace gas measurements, as well as continuous measurements of aerosol optical properties and condensation nuclei concentrations have been conducted for a number of years. However, this station is not representative of the inland/sub-continental southern Africa, especially for modelling validation, since the dominant wind direction is from the open sea. Therefore, the Cape

Point GAW station is making it more useful as a Southern Hemisphere marine background site.

For South Africa, there are also a limited number of studies considering cloud condensation nuclei (CCN) (Ross et al., 2003; Laakso et al., 2013), as well as optical and chemical properties of aerosols. These measurements were mainly performed during the SAFARI 1992 (Fishman et al., 1996; Lindesay et al., 1996) and SAFARI 2000 measurement campaigns (Eautough et al., 2013; Kirchstetter et al., 2003; Swap et al., 2003), as well as the EUCAARI campaign from 2009 to 2011 (Laakso et al., 2012, 2013). The main findings from these campaigns highlighted the importance of regional circulation, seasonal variation, multiple inversion layers (especially strong winter-time inversions) and the mixture of anthropogenic sources including domestic burning, wild fires and industry. High O_3 concentrations were found to be the most likely to cause adverse environmental effects (Zunckel et al., 2004).

During the above-mentioned intensive campaigns, the majority of aerosol chemistry studies were based on filter sampling, with associated low time resolution and rather large particle size cuts (TSP, PM$_{10}$ and PM$_{2.5}$). A limited number of ultrafine aerosol studies have been published (Laakso et al., 2008; Hirsikko et al., 2013; Vakkari et al., 2011, 2013) based on the data obtained from a relative clean savannah site and an industrial site in South Africa (Hirsikko et al., 2012). At these sites, atmospheric new particle formation and growth events were observed during almost all sunny days and these events were influenced both by local and regional pollution sources. The same studies indicated high levels of Aitken and accumulation mode particles originating from domestic household combustion associated with space heating and cooking during the mornings and evenings.

Secondary organic aerosols (SOA), formed by condensation of low-volatility products of the oxidation of hydrocarbons, usually contribute significantly to the total atmospheric organic aerosols (OA) (Jimenez et al., 2009). Secondary inorganic ions (sulphate, nitrate and ammonium) together with OA dominate the mass of sub-micron aerosols downwind of anthropogenic fossil fuel burning sources emitting SO_2 and NO_x. Biomass burning processes generate significant amount of aerosols over southern Africa in the dry season and also emit significant amount of different trace gases (Swap et al., 2003).

Organic compounds constitute a large fraction of submicron particle mass at the global scale (Kanakidou et al., 2005). Therefore, their accurate quantification and source apportionment are necessary in order to determine their role in the atmosphere. The study of OA in the atmosphere is challenging due to the large number of molecular species involved and the continuous evolution of OA concentration, composition, and properties (Jimenez et al., 2009). Recently, simplified analytical methods to characterise OA and its aging have been developed (Ng et al., 2010). In particular, positive matrix factorization (PMF) of aerosol mass spectrometer

(AMS) mass spectra has been applied to characterise sources and transformation of OA in the atmosphere (Zhang et al., 2005a, 2011; Lanz et al., 2007; Ulbrich et al., 2009).

In this manuscript, we analyse aerosol measurements made at the Welgegund monitoring station in South Africa. The station is ideally located for investigating oxidized OA and biomass burning organic aerosols (BBOA), since there are no significant OA sources nearby. The site is also strategically positioned for monitoring air masses passing over the regional background, as well as influences from major anthropogenic source areas in the interior of South Africa. In this paper, we will interpret submicron chemical composition of aerosol measurements by using meteorological measurements, air mass backtrajectories and other complementary measurements conducted at Welgegund. Our results provide an overview of sub-micrometer chemical composition in southern Africa in both the wet and dry seasons and give insight into sources, as well as atmospheric processes of organic aerosols. Prior to this study, no long-term high time resolution aerosol chemical composition measurements have been conducted in southern Africa.

2 Methods

2.1 Site description

The Welgegund measurement site presented in Fig. 1 (26°34′10″ S, 26°56′21″ E, 1480 m a.s.l.) (http://www.welgegund.org; Beukes et al., 2014) is located approximately 100 km southwest of the Johannesburg-Pretoria conurbation with a population of over 10 million (Lourens et al., 2012). There are no major local pollution sources close to the measurement site. However, it is frequently impacted by air masses with pollution plumes from the Johannesburg-Pretoria megacity, the industrialised western and eastern Bushveld Igneous Complex, the Vaal Triangle and the industrialised Mpumalanga Highveld. Beukes et al. (2014) give an overview of these anthropogenic source regions. Air masses, passing over the clean background toward the west of Welgegund where no significant point sources occur, also regularly arrive at Welgegund.

The large-scale meteorology in the region is characterised by a high degree of stability and anti-cyclonic circulation (Garstang et al., 1996; Tyson and Preston-Whyte, 2000). Due to limited vertical mixing, the atmosphere is often layered, containing clean and polluted horizontal cells (Hobbs, 2003). This limited vertical mixing, together with the relatively high stack heights of the major point sources and anti-cyclonic circulation, frequently result in air masses that are contaminated to some degree by either industrial sources or biomass burning. Under specific synoptic conditions, air re-circulates over the sub-continent for up to 20 days (Garstang et al., 1996; Tyson and Preston-Whyte, 2000; Swap et al., 2003). Land-cover surrounding the Welgegund measurement station is grassland savannah, grazed by cattle and sheep (Beukes et al., 2014).

2.2 Instrumentation

Measurements were carried out with a mobile atmospheric monitoring trailer (Petäjä et al., 2013), that was permanently placed at Welgegund in May 2010. Ancillary data included gas concentrations and basic meteorological parameters (see Beukes et al., 2014 and Petäjä et al., 2013 for a full list of measurements conducted at Welgegund). Local meteorological parameters included temperature, relative humidity (RH), wind speed and direction, photosynthetically active radiation (PAR) and precipitation. Temperature and RH were measured with a Rotronic MP 101A instrument, while wind speed and direction were measured with the Vector A101ML and A200P/L, respectively. O$_3$, SO$_2$, NO$_x$ and CO concentrations were measured with an Environment S.A. O341M, a Thermo 42S, a Teledyne Instruments 200AU and a Horiba APMA-360 instruments, respectively. Ambient PM$_1$ concentrations were measured using synchronized hybrid ambient real-time particulate monitor SHARP 5010 (Thermo Electron Corporation) and black carbon (BC) was measured with a continuous multiangle absorption photometer MAAP (Thermo Electron Corporation).

Particle size distributions were measured with a differential mobility particle sizer (DMPS) system with a size range of 12–840 nm (Wiedensohler, 1988). The dried sample (Nafion drier, Perma Pure LLC, USA) was drawn through and classified with Vienna-type differential mobility analyser (DMA, Winklmayr et al., 1991) and counted with a TSI condensation particle counter (Model 3010 CPC, time resolution of 9 min). All instruments were checked and maintained at least once a week and data was downloaded automatically to a server every day at 00:00 local time (LT). All raw data were cleaned before data analyses, according to methods described by Laakso et al. (2008), Vakkari et al. (2011), Venter et al. (2012) and Hirsikko et al. (2012).

The chemical composition of Aitken and accumulation aerosol particles was analysed on-line and in real-time with an Aerosol Chemical Specification Monitor (ACSM, Aerodyne Inc.). The ACSM is designed for continuous long-term measurements of the chemical composition of non-refractory submicron PM and is based on the same technology as the Aerosol Mass Spectrometers (AMS) (Jayne et al., 2000; DeCarlo et al., 2006; Ng et al., 2011a). The sample flow was passed through a PM$_1$ cut-off impactor, where after it was conducted to the ACSM using an additional pump with a flow of 3 L min^{-1}. Particles were drawn into the ACSM through a 100 μm critical orifice ($\sim$ 0.09 L min^{-1}) to an aerodynamic lens assembly (Liu et al., 1995). The aerodynamic lens with D_{50} limits of 75 nm and 650 nm (Liu et al., 2007) focused particles into a narrow beam that is directed through two vacuum chambers to an ionization chamber. The particle beam was directed onto a heated conical porous tungsten
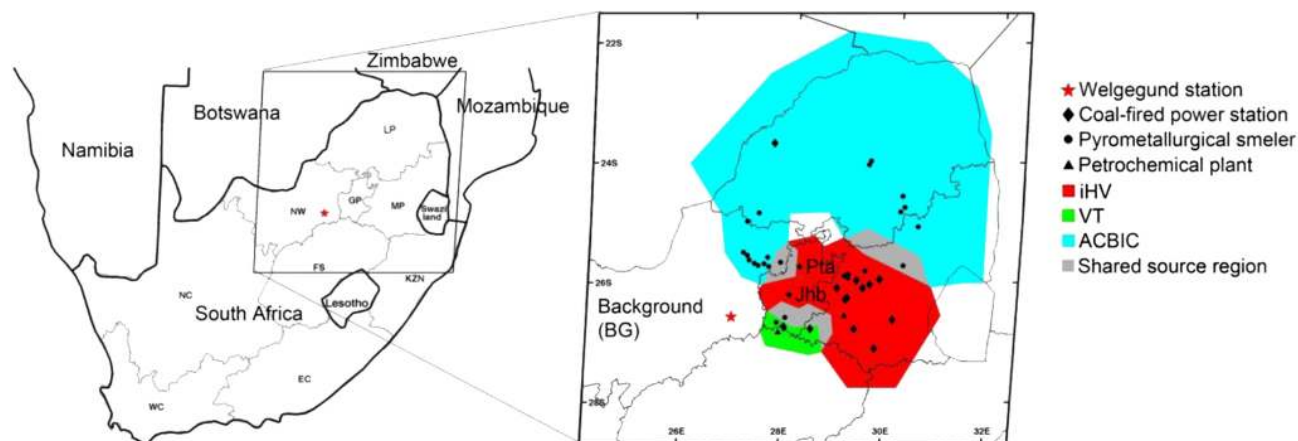
Fig. 1. Location of the Welgegund measuring site (marked as red star) and major source regions marked with colours. The grey areas on this map indicate where there is a likelihood that the various source regions overlap. Trajectories passing over these regions of uncertainty were rejected (see Beukes et al. (2014) for details).

surface (600 °C) at the centre of the ionization chamber. Here aerosol components flash-vaporized and the vaporized molecules were ionized by electron impact (70 eV). Non-refractory (NR) material in this paper is defined as the particulate material that vaporizes at 600 °C (e.g., DeCarlo et al., 2006). Positive ions were detected with a mass spectrometer (MS) equipped with a residual gas analyser (RGA) type quadrupole mass analyser (Pfeiffer Vacuum GmbH).

The MS scan rate was set to 0.5 m/z per second and alternate MS scans sampled ambient air passing through a particle filter to provide an MS blank. Using a 30 min averaging time, 3σ detection limits for ammonium (NH$_4^+$), organics, sulfate (SO$_4^{2-}$), nitrate (NO$_3^-$) and chloride (Cl$^-$) were 0.284 µg m^{-3}, 0.148 µg m^{-3}, 0.024 µg m^{-3}, 0.012 µg m^{-3} and 0.011 µg m^{-3}, respectively (Ng et al., 2011a).

An internal naphthalene signal (m/z 128) and the air ion signals from the reference state was used to monitor variability in overall instrument performance, as well as changes due to variation in the sampling flow rate (air only). Frequent power outages interrupted a number of measurement days and temporarily decreased ion transmission efficiency of heavier masses that included naphthalene. For this reason all zero naphthalene signal periods were deleted from further analysis. The detailed description of the instrument, associated calibrations, data correction procedures and operation procedures are presented in Ng et al. (2011a).

Aerosol mass concentrations also need to be corrected for the particle collection efficiency (CE). The values of CE can be smaller than 1 because of losses in the vaporizer or aerodynamic inlet. Particle collection losses in the vaporizer, result from inefficient focusing of non-spherical particles onto the vaporizer or due to bouncing of solid particles before they are completely vaporized. Particle losses in the aerodynamic inlet are a function of particle diameter and are relatively well characterised (Huffman et al., 2005; Liu et al., 2007;

Matthew et al,. 2008). Current ACSM systems use aerodynamic lens and vaporizer designs identical to those in the AMS, so we expect CE values to be similar to those observed in AMS measurements. The database of AMS field results indicates that a CE value of 0.5 is found to be representative with data uncertainties of $\pm20\%$ (Canagaratna et al., 2007). Recent studies have shown that CE values may be influenced by factors such as particle phase, composition and water content (e.g., Matthew et al., 2008). The correction algorithm developed by Middlebrook et al. (2012) was used in this study. The CE for the ambient aerosol measurements in this sampling campaign ranged from 0.45 to 0.83 with a mean of 0.46.

For quantitative ACSM measurements, the ionization efficiency (IE) was determined by calibration with 300 nm ammonium nitrate (NH$_4$NO$_3$) particles (Jayne et al., 2000). Dried and size-selected NH$_4$NO$_3$ particles were measured with the ACSM and a CPC (TSI 3010, Mertes et al., 1995) in parallel. NH$_4$NO$_3$ calibration allows for the determination of other compounds in terms of NO$_3^-$ equivalent mass using the relative ionization efficiency (RIE). RIE values of 3.8, 1.4 , 1.2 , 1.1 and 1.3 were used for NH$_4^+$, organic species, SO$_4^{2-}$, NO$_3^-$ and Cl$^-$, respectively (Allan et al., 2003; Jimenez et al., 2003). All mass concentrations presented in this paper were determined at ambient temperature and pressure (local pressure is approximately 850 kPa) and presented in local time. Additionally aerosol data was cleaned by visually inspection. Periods and size intervals when data was noisy or otherwise suspicious were removed from the dataset, such as time periods right after power breaks before ACSM performance was stabilized.

Figure 2 shows a comparison between the combined total aerosol mass obtained from the ACSM (calculated with the time-depend CE values) and BC, in comparison with corresponding mass calculated from DMPS measurements.
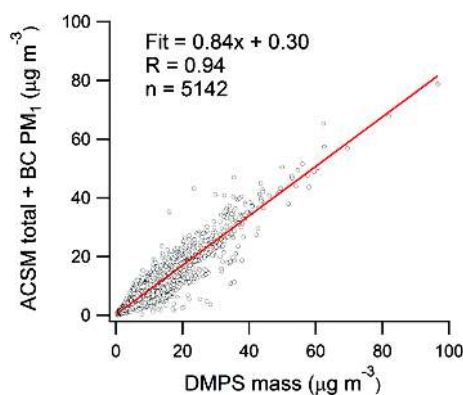
Fig. 2. Scatter plot of NR-PM$_1$ + BC mass vs. calculated DMPS mass.

The latter were obtained by converting the particle number size distributions measured by the DMPS to the volume distributions assuming spherical particles and multiplying the total particle volume concentration by the estimated mean particle density of 1.88 g cm^{-3}. The average particle density was estimated by comparing DMPS volumes to the carefully-checked, real-time PM$_1$ particulate monitor masses (10881 data points). The sum of the total ACSM mass and BC concentration correlated well with the mass concentration calculated from the DMPS measurements with a correlation coefficient of 0.94. The ACSM does not detect aerosol components that vaporize at temperature higher than 600 °C. These aerosols include BC, crustal oxides, potassium chloride (KCl), non-volatile organics and sea salt (refractory material).

Fitting of the data in Fig. 2 gives a semi-empirical estimate of the average mass of refractory material, M:

$$\begin{cases} \text{ACSM} + \text{BC} = 0.84 \times \text{DMPS} + 0.3 \\ M + \text{BC} = \text{DMPS} - \text{ACSM} \end{cases} \tag{1}$$

$$\Rightarrow M = 0.19(\text{ACSM} + \text{BC}) - 0.36 \tag{2}$$

Here M + BC describe the annual-average non-volatile fraction of the PM$_1$ mass.

2.3 Factor analysis

PMF is a statistical source apportionment tool that uses constrained, weighted least squares estimation to determine source profiles and strengths. Specifically, PMF is a variant of a factor analysis method with non-negative factor elements and it takes into account error estimations of observed data values (Paatero and Tapper, 1994; Paatero, 1997). PMF has been applied recently on many organic mass spectra measured by AMS, mainly in the Northern Hemisphere (Ng et al., 2010; Zhang et al., 2011).

The analysis utilised version 4.2 of the PMF2 algorithm on robust mode (Paatero and Tapper, 1994; Paatero, 1997), applying the PMF Evaluation Tool v.2.04 (Ulbrich et al.,

2009). Standard data pre-treatment, including applying minimum error criteria, down-weighting weak variables and m/z 44 related peaks, was performed as described in Ulbrich et al. (2009). Additionally, scaled residuals were examined carefully. Species with > 10 % of scaled residuals larger than $\pm 2\sigma$ were re-weighted by a factor ranging between 2–5 until the above criteria was satisfied so that m/z 60 and m/z 117 were down-weighted by a factor of three. The m/z 12 was excluded, since re-weighting did not improve residuals. Extreme concentration peaks, which could disturb analysis, were down-weighted by a factor of 10. These peaks were mainly caused by savannah fires and lasted 4–6 h.

2.4 Trajectories

The air mass history was investigated using backtrajectories calculated with the HYbrid Single-Particle Lagrangian Integrated Trajectory (HYSPLIT) version 4.8 model developed by the National Oceanic and Atmospheric Administration (NOAA) Air Resources Laboratory (ARL) (Draxler and Hess, 2004). The model ran with the GDAS meteorological archive produced by the US National Weather Service's National Centre for Environmental Prediction (NCEP) and archived by ARL (Air Resources Laboratory, 2012). 96 h backtrajectories were obtained for every hour throughout the complete measurement period with an arrival height of 100 m. Backtrajectory accuracy greatly depends on the quality of the underlying meteorological data (Stohl, 1998). The errors accompanying single trajectories are currently estimated as 15 to 30 % of the backtrajectory distance travelled (Stohl, 1998; Riddle et al., 2006).

2.5 Source regions

In this the measurements at Welgegund were classified into four source regions based on air mass history. The source regions recently defined for Welgegund by Beukes et al. (2014) were used for this purpose in simplified form. Since these source regions were discussed in detail by Beukes et al. (2014), these source regions are only briefly introduced here. The source region characterisation presented will examine the influences of four major source sector (Fig. 1), which are subsequently introduced:

– ACBIC: most of the air masses arriving at Welgegund pass over an area that mimics the anti-cyclonic recirculation of air masses over the South African interior. Therefore, this anti-cyclonic recirculation path forms a clearly identified source region, as pollutants emitted in the primary source region are recirculated. This allows for pollutants to become aged and undergo various chemical reactions. However, within the accuracy of backtrajectory calculations (Sect. 2.4), the anti-cyclonic source region of Welgegund significantly overlaps with the western and eastern Bushveld Igneous Complexes. A large fraction of the mineral

assets of South Africa (e.g., Cramer et al., 2004) is concentrated in the Bushveld Complex (BIC), with the western limb being the most exploited (see Hirsikko et al., 2012). Due to the lure of employment, the western BIC is populated by formal (larger cities and towns, such as Rustenburg and Brits), semi-formal and informal settlements. Incomplete combustion of coal and wood in ineffective appliances for household heating and cooking are common occurrences in the semi-formal and informal settlement sectors (Venter et al., 2012). Due to the geographical overlap of the aforementioned source regions, i.e., the anti-cyclonic, western and eastern BIC source regions, these three source regions were combined in this paper as a single source region, referred to as ACBIC.

– VT: the highly industrialised and relatively densely populated Vaal Triangle (VT) source region contains various large point sources, including petrochemical and metallurgical industries. Although the geographical definition of this source region does not correlate perfectly with classifications currently used in South African air quality legislation, the Vaal Triangle area has been declared an air pollution hotspot in South Africa.

– iHV: the Industrial Highveld (iHV) source region defined here extends from the eastern parts of the Gauteng province, north to Middelburg in the Mpumalanga Province. This source region (iHV) is actually a combination of two large source regions, i.e., the Mpumalanga Highveld where 11 coal fired power stations and a large petrochemical plant occur within a 60 km radius, as well as the Johannesburg-Pretoria megacity with more than 10 million inhabitants (Lourens et al., 2012). Beukes et al. (2014) treated these regions more detail. This combined source region (iHV) is a major source of NO$_x$ (Lourens et al., 2012).

– BG: the regional background (BG), containing no large point sources, is located west from the Welgegund measurement site. This includes portions of the North-West and the Free State provinces, as well as the entire Northern Cape province of South Africa. The Northern Cape is the most sparsely populated province in South Africa, with less than 10 inhabitants per km^2. The BG source region also included the Kalahari desert. Although the BG source region contained virtually no large point sources, local and regional biomass burning do occur during the dry season.
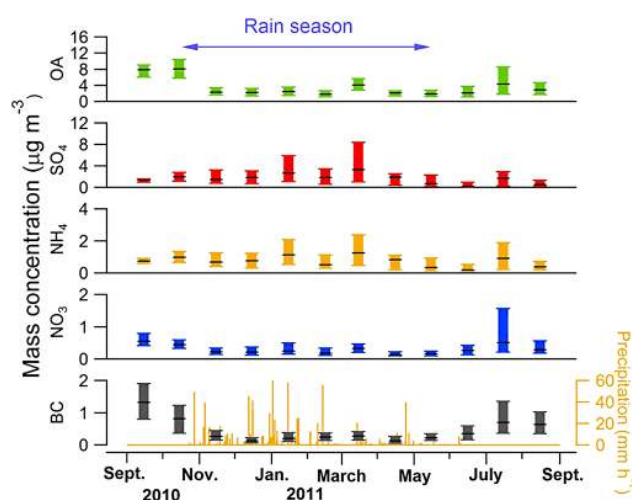
Fig. 3. Monthly median concentrations of OA, SO$_4^{2-}$, NH$_4^+$, NO$_3^-$ and BC, as well as rainfall intensities. The box plots indicate median, as well as 25th and 75th percentiles.

3 Results and discussion

3.1 Meteorology

Local weather conditions were categorized in two main periods: (1) the warm and wet rainy season from mid-October to mid-May, during which time frequent precipitation occurs and (2) the colder and dry season from mid May until mid October during which time almost no precipitation occurs (Fig. 3). The mean temperature during the sampling period was 17.2 °C, with a maximum of 34.4 °C and a minimum temperature of −2.7 °C. Wind directions were primarily from the northerly and northwesterly directions, with mean wind speed of 5.5 m s^{-1}. The mean atmospheric pressure measured was 852 hPa (min. 844 hPa, max. 863 hPa).

3.2 Mass concentrations, composition and diurnal variation of aerosols

ACSM measurements were carried out from 1 September 2010 to 16 August 2011. The total mass concentration of NR-PM$_1$ varied substantially during the measurement campaign from less than 1 μg m^{-3} to about 89 μg m^{-3} with a mean of 7.5 μg m^{-3} (Table 1). The highest concentrations were usually observed during stable atmospheric conditions with polluted air masses caused by regional or local biomass burning episodes, or in air-masses transported from iHV source region. Quite often such polluted conditions were followed by quick drops in the PM$_1$ mass concentration associated with heavy rains and/or frontal systems from the west that are associated with relatively clean air masses. The measured PM$_1$ mass concentrations levels were quite similar to those observed in a suburban area in New York City (Sun et al., 2011), in Finokalia, Greece (Hildebrandt et al., 2010) and

in Cabauw, the Netherlands (Mensah et al., 2012). Concentrations were, however, lower than those in the Mexico City metropolitan (Salcedo et al., 2006) or in Beijing (Sun et al., 2010).

Figure 3 shows the monthly average concentrations of OA, SO$_4^{2-}$, NH$_4^+$, NO$_3^-$ and BC, together with the frequency of precipitation events. Statistical data of the mass concentrations of each species measured in the sampling period are listed in Table 1. The NR-PM$_1$ aerosol composition was dominated by OA (48 %) and SO$_4^{2-}$ (33 %), while the mean observed fractions of NH$_4^+$ and NO$_3^-$ were 13 % and 6 %, respectively. Chloride (Cl$^-$) concentrations were generally low contributing to less than 1 % of total NR-PM$_1$ and were near the ACSM detection limit of 11 ng m^{-3}.

The highest OA concentrations were observed during the dry season when it peaked at levels of up to 75 µg m^{-3} as a result of regional and local savannah fires. The highest SO$_4^{2-}$ concentrations (max. 27 µg m^{-3}) were observed in air mass originating from the eastern highly populated and industrialised areas, i.e., in air masses that had passed over the iHV source region (see Fig. 1 for iHV spatial definition). Refractory PM$_1$ mass, excluding BC, was estimated from Eq. (1) as having a mean loading of 1.2 µg m^{-3}, whereas the mean BC concentration was 0.5 µg m^{-3}. During the dry season, the BC concentration peaked almost simultaneously with OA and reached concentrations up to 10 µg m^{-3}. The mean estimated total PM$_1$ mass fractions were 39 %, 27 %, 10 %, 5 %, 1 %, 5 %, 13 % for OA, SO$_4^{2-}$ NH$_4^+$ NO$_3^-$, Cl$^-$, BC and refractory material, respectively, and the mean total loading of PM$_1$ mass was 9.1 µg m^{-3}.

The monthly-average concentrations of OA varied in the range of 2–8 µg m^{-3}. The concentrations showed a clear seasonal pattern characterised by higher and more disperse values during the dry season than during the wet season. NO$_3^-$ concentrations had a similar seasonal pattern to OA, with monthly-average values in the range of 0.2–0.5 µg m^{-3}. NO$_3^-$ was a minor PM constituent, except in July when it is comparable to SO$_4^{-2}$ and NH$_4^+$. These simultaneously high levels of the OA, NO$_3^-$ and BC in the dry season are attributable to biomass burning episodes that are frequent at this time of the year in southern Africa (e.g., Swap et al., 2003). More detailed analyses of biomass burning episodes are presented in Vakkari et al. (2014).

The highest and most dispersed concentrations for SO$_4^{2-}$ were found in the late wet season when the SO$_4^{2-}$ mass fraction was twice that in the dry season. The SO$_4^{2-}$ concentrations exceeded those of OA frequently during March, especially when the air-masses had passed over iHV, where the majority of coal-fired power plants are located (Siversten et al., 1995). At least two factors contributed to the high SO$_4^{2-}$ concentrations during the wet season: the more frequent exposure to easterly air masses affected by the iHV area with high SO$_2$ emissions and the frequent presence of clouds which tends to enhance SO$_4^{2-}$ formation by in-cloud
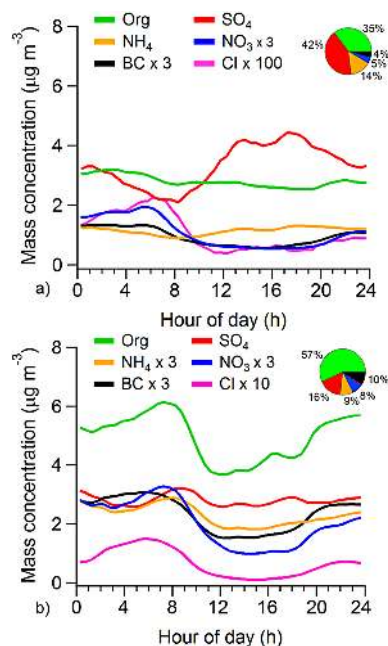
Fig. 4. Diurnal cycle of OA, SO$_4^{2-}$, NH$_4^+$, NO$_3^-$ and BC, in both the wet **(a)** and the dry **(b)** seasons. NO$_3^-$ and BC concentrations were multiplied by 3 and Cl$^-$ by 10/100 for scaling. Mean compositions are shown in the pie charts (percentages).

SO$_2$ oxidation (Shen et al., 2012). Concentrations of NH$_4^+$ varied from 0.2 to 1.1 µg m^{-3} and correlated well with those of sulfate ($R = 0.89$), especially during the dry season, indicating the presence of ammonium sulfate in ambient air. Ammonium concentrations will be discussed in more detail in Sect. 3.3.

Figure 4a and b show the diurnal cycles of the mass concentrations of the major aerosol constituents in the wet and dry seasons, respectively. Unlike the other constituents, SO$_4^{2-}$ had a pronounced diurnal profile in the wet season, peaking during the late afternoon. The most likely explanation for this was the breakup of the inversion layer(s) during daytime, which increased the height of the surface mixed layer and entrainment of air from above. In this way, the high-stack emitted SO$_2$ and its oxidation product SO$_4^{2-}$ could be brought more efficiently down to the surface. The more efficient mixing during the daytime may also have accelerated the oxidation of SO$_2$ to SO$_4^{2-}$ by more efficient in-cloud processing of the air, but this phenomenon cannot be verified with our surface measurements.

During the dry season, concentrations of OA, NO$_3^-$ and BC dropped sharply after the inversion layer break-up in the morning hours, indicating low level and relatively localized sources (i.e., savannah fires) for these compounds. Their concentrations tended to increase toward the night due to lower boundary layer heights that limit mixing.

The similar diurnal patterns for NO$_3^-$ and Cl$^-$ were expected because both these species are sensitive to the ambient

Table 1. Statistics of mass concentrations (µg m^{-3}) of the NR-PM$_1$ compounds, BC and total PM$_1$.

	Mean	Median	25th percentiles	75th percentiles	Max
OA	3.6	2.6	1.5	4.4	75.2
SO$_4^{2-}$	2.4	1.5	0.4	3.2	27.2
NH$_4^+$	0.9	0.7	0.3	1.3	7.2
NO$_3^-$	0.5	0.3	0.1	0.4	11.1
Cl$^-$	0.03	< DL	< DL	0.03	2.6
BC	0.5	0.3	0.2	0.6	11.4
Total NR-PM$_1$	7.5	5.6	2.8	10.3	89
Total NR-PM$_1$ + BC	8.0	6.0	3.0	11.0	96
Total PM$_1$	9.1	6.8	3.3	12.8	113

temperature and relative humidity. The diurnal cycle of NO$_3^-$ is driven by HNO$_3$ production and gas-to-particle partitioning to ammonium nitrate (NH$_4$NO$_3$), the latter of which is controlled by the temperature and relative humidity (Seinfeld and Pandis, 2006). A diurnal nitrate concentration cycle quite similar to ours has been observed in New York (Sun et al., 2011) and Pittsburg (Zhang et al., 2005b). Similarity of the diurnal cycle of NH$_4^+$ to that of SO$_4^{2-}$ during the wet season occurred because NH$_4^+$ was mainly in the form of (NH$_4$)$_2$SO$_4$, whereas during the dry season diurnal variation of NH$_4^+$ resulted from the combination of the diurnal cycles of particulate (NH$_4$)$_2$SO$_4$ and NH$_4$NO$_3$.

3.3 Acidity of submicron particles

The acidity of atmospheric aerosol particles influences their hygroscopicity and their ability to produce heterogeneous sulfate and SOA (Liang and Jacobson, 1999; Jang et al., 2002; Martin et al., 2003; Pathak et al., 2011). It is possible to estimate the acidity of NR-PM$_1$ by comparing the measured NH$_4^+$ mass concentration to the amount of NH$_4^+$ needed to completely neutralize the anions that were calculated using Eq. (3):

$$NH_{4,cal}^+ = 18 \times \left(2 \times \frac{SO_4^{2-}}{96} + \frac{NO_3^-}{62} + \frac{Cl^-}{35.5} \right) \qquad (3)$$

Here SO$_4^{2-}$, NO$_3^-$ and Cl$^-$ are the mass concentration of the ions (µg m^{-3}) and the denominators correspond to their molecular weights, with 18 being the molecular weight of NH$_4^+$. Particles are considered to be "more acidic" if the measured NH$_4^+$ concentration is significantly lower than the calculated and as "bulk neutralized" if the two values are equal. This approach is valid if the influence of metal ions, as well as organic acids and bases on NH$_4^+$ concentration is negligible (Zhang et al., 2007b). When the sulfate to NH$_4^+$ ratio is high, the amount of atmospheric ammonium is not sufficient to neutralize all SO$_4^{2-}$, NO$_3^-$ and Cl$^-$ anions. In such a case at least a fraction of NO$_3^-$ and Cl$^-$ anions must be associated

with cations other than NH$_4^+$ and Eq. (3) is no longer valid. Thus, the amount of NH$_4^+$ needed to completely neutralize SO$_4^{2-}$ can be calculated from the following equation:

$$NH_{4,cal,SO_4^{2-}}^+ = 18 \times \left(2 \times \frac{SO_4^{2-}}{96} \right) \qquad (4)$$

For dry season, the correlation between measured and calculated NH$_4^+$ was excellent with a regression slope near 1 ($R = 0.97$) (Eq. 3, Fig. 5a), indicating that NR-PM$_1$ in Welgegund was mainly neutralized. Contrary to that, the wet season showed a much lower correlation slope ($R = 0.70$) (Fig. 5b) even with Eq. (4), in which other species than SO$_4^{2-}$ are ignored. Therefore the amount of NH$_4^+$ in submicron particles was insufficient to neutralize SO$_4^{2-}$ in the wet season. However, the slope is near unity when SO$_4^{2-}$ concentration was lower than ~ 2 µg m^{-3} so acidic aerosols were not observed when SO$_4^{2-}$ concentration was low.

Furthermore, the results implies that a fraction of the observed NO$_3^-$ and Cl$^-$ was very likely associated with either potassium originating from biomass burning or metal-containing particles. It can be assumed that the numerous large point sources in this region (Fig. 1) add metal-containing particulates to the local and regional atmosphere.

3.4 Source region characterisation

Calculated backtrajectories were classified as passing over the various source regions defined in Sect. 2.5. Mean concentrations for all measured compounds were calculated for air masses that had passes over each source region (Figs. 6 and 7, Table 2) for both the dry and the wet season. In addition to that, Fig. S1 (Supplement) present source area maps for different mass components. The maps have been generated with the simple approach used by Vakkari et al. (2011, 2013), where point measurements are connected to 96 h HYSPLIT (Draxler and Hess, 2004) backtrajectories to gain an overview of regional scale patterns.

As expected, the mass concentrations were the lowest when air masses passed over the relatively clean BG region
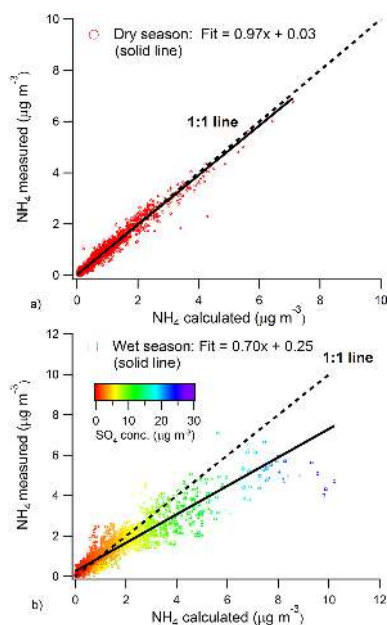
Fig. 5. Measured vs. calculated NH$_4^+$ and linear fittings (solid lines) using **(a)** Eq. (3) (dry season) and **(b)** Eq. (4) (wet season). Data points **(b)** are colour-coded according to SO$_4^2$ concentration.

Table 2. Summary of mean mass concentrations (μg m^{-3}) of the NR-PM$_1$ compounds and BC for four main source regions both dry and wet seasons (dry/wet).

	BG	VT	iHV	ACBIC
OA	2.3/2.0	4.5/2.9	10.5/3.0	6.8/2.4
SO$_4^{2-}$	0.4/1.4	1.3/4.3	2.5/3.9	2.2/2.7
NH$_4^+$	0.3/0.5	1.0/1.5	1.9/1.3	1.0/1.0
NO$_3^-$	0.3/0.2	1.5/0.5	2.9/0.4	0.5/0.2
Cl$^-$	0.04/–	0.1/–	0.3/–	0.05/–
BC	0.6/0.3	1.3/0.5	1.5/0.4	1.1/0.3
Total + BC	3.8/4.4	9.7/9.6	19.7/9.1	11.7/6.5

(Figs. 6 and 7, Table 2) and the highest for the iHV region. The iHV air masses also showed the highest variability of concentrations (Fig. 6).

Compared with the wet season, concentrations of OA, NO$_3^-$ and Cl$^-$ were higher during the dry seasons for all air masses passing over all the defined source regions (Figs. 6 and 7). In contrast to that, SO$_4^{2-}$ concentrations were higher during the wet season for all regions. This indicates that enhanced SO$_4^{2-}$ concentration is not only due to emissions from the iHV region, but also due to other factors like the in-cloud oxidation of SO$_2$ to SO$_4^{2-}$ as discussed earlier. Furthermore, during the wet season the cleanest air masses from the southwestern Karoo region were absent (Fig. S1) and therefore the wet season BG region was more affected by aged regional air masses with higher SO$_4^{2-}$ concentrations.
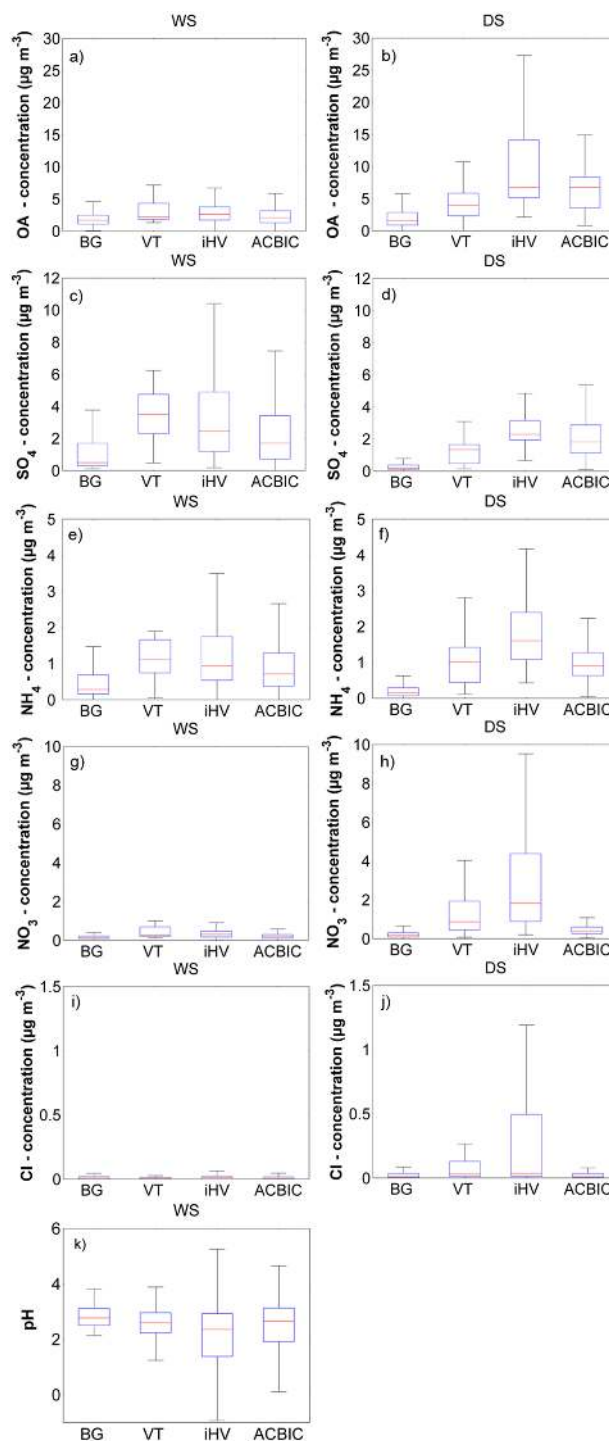
Fig. 6. NR-PM$_1$ composition as function of air masses classified as passing over the four regions, i.e., BG, VT, iHV and ACBIC, defined in Sect. 2.5 for the wet season (WS) and the dry season (DS) as well as pH for WS (*k*). The box plots indicate 25th and 75th percentiles and the line within the box the median. Whiskers present 5th and 95th percentiles.

The concentration of NH_4^+ showed more variability between the seasons than the concentrations of other compounds (Fig. 6e and f). The iHV-related NH_4^+ concentration was higher in the dry season while the BG- and VT-related NH_4^+ concentrations were higher in the wet season. Petrochemical industries are quite prevalent in the VT (Beukes et al., 2014). It is possible that these industries contribute significantly to high ammonium emissions. The nitrate concentrations were the highest from the iHV and VT regions, which is consistent with recent findings by Lourens et al. (2011, 2012) that these areas have high NO_x emissions due to high traffic densities and large point sources. Interestingly, for the air masses that have passed over iHV (Fig. 6j) Cl^- content peaked only during dry season indicating combustion related emissions like coal combustion (Zhang et al., 2012), waste combustion (e.g., Moffet et al., 2008) or local savanna fires (e.g., Akagi al., 2012) but according this dataset exact combustion source cannot be verified.

Aerosol acidity was calculated using Aerosol Inorganic Model II (AIM-II) with gas-aerosol interaction disabled (Clegg et al., 1998). Measured concentrations of SO_4^{2-}, NO_3^-, NH_4^+, ambient temperature (T) and relative humidity (RH) were used as inputs and only the acidic aerosols were considered. pH values were calculate using equation

$$pH = -\log(fH_{aq}^+ \times xH_{aq}^+) \tag{5}$$

where fH_{aq}^+ is the mole fraction based activity coefficient of hydrogen ions and xH_{aq}^+ is the equilibrium mole fraction of hydrogen ions in the particles (Zhang et al., 2007b). It has to be noted that we have neglected the influence of organics on hydration and the thermodynamical equilibrium of inorganic ions. The organics are expected to have only a minor effect on partitioning/dissociation of inorganic species in acidic particles (Zhang et al., 2007b).

Aerosols were mainly neutralized for BG and ACBIC regions when 10 % and 23 % of data points were acid (wet season), whereas 46 % of iHV and 63 % of VT regions data points were classified as acid aerosols defined in Sect. 3.3. Average pH values of acidic aerosols calculated from Eq. (5) were between 2.1 and 2.6 with minimum pH of -0.93 (Fig. 6k).

3.5 Organic aerosols

Atmospheric OA are generally separated in two main types of compounds, i.e., hydrocarbon organic aerosols (fresh emissions) and oxygenated organic aerosols (OOA), which usually dominate the total organic mass (Allan et al., 2004; Zhang et al., 2005a; Canagaratna et al., 2007). OOA can, in most environments, be further divided into low-volatile, highly oxidized OOA (LV-OOA) and semi-volatile OOA (SV-OOA) (e.g., Jimenez et al., 2009). The mass spectra of LV-OOA are associated with a higher peak at m/z 44 as a result of the presence of CO_2^+. Previous studies have shown that the CO_2^+ fragment in the OA spectra can result from

thermal decarboxylation of organic acids (e.g., Alfarra et al., 2004; Aiken et al., 2007), whereas the mass spectra of SV-OOA is dominated by the $C_2H_3O^+$ ion (m/z 43), which is an indicator of non-acid oxygenates (e.g., Ng et al., 2010).

A significant fraction of the NR-PM$_1$ aerosols measured at the Welgegund site consisted of OA (63 % of total OA in dry season and 37 % in wet season). The organic composition differed and the concentration levels varied considerably between seasons, due to different sources (e.g., savanna fires and biogenic organics) and atmospheric conditions (e.g., water content). To better understand the chemical composition and sources of OA, oxidation levels of OA and ACSM mass spectra of OA are discussed in more detail below.

3.5.1 PMF analysis of OA

Insight into the oxidation level of OA can be obtained from the analysis of the ACSM mass spectra through the use of PMF (Zhang et al., 2005a, 2011; Ulbrich et al., 2009). In this study, we applied PMF to characterise the organic aerosol content and moreover to identify organics groups, their time-dependent concentrations and mass spectra (MS) from the OA dataset. All PMF analysis details are presented in Zhang et al. (2005a, 2011) and Ulbrich et al. (2009). The OA MS showed the characteristic features of oxidized material, e.g., the major peaks of m/z 44 (CO_2^+). The differences in intensity of m/z 44 and m/z 43 fragments reveal levels of oxidation in OOA components (e.g., Sun et al., 2010).

The 2-factor PMF separated oxygenated organic aerosols (OOA) and primary biomass burning organic aerosol (BBOA) with Q/Q_{exp} (Ulbrich et al., 2009) of 1.33. The 3-factor solution indicated BBOA, SV-OOA and LV-OOA ($Q/Q_{exp} = 1.23$). The 4-factor solution split the LV-OOA factor into two separate factors ($Q/Q_{exp} = 1.13$). The 5-factor solution further split the LV-OOA ($Q/Q_{exp} = 1.06$), but these factors were almost identical to LV-OOA ($R > 0.95$).

Because of the distinguishable differences in atmospheric conditions (e.g., water content) and sources (e.g., savanna fire emissions) between the dry and wet seasons (e.g., Laakso et al., 2013), the PMF analyses were conducted separately for these two seasons. In this case, the dry season solution showed two factors, i.e., OOA and BBOA with Q/Q_{exp} of 1.26 (Fig. 8b). The two OOA profiles obtained with the 3-factor profiles ($Q/Q_{exp} = 1.08$) were identical ($R = 0.98$). For the wet season no distinct BBOA factor was identified, whereas both LV-OOA and SV-OOA were obtained ($Q/Q_{exp} = 1.19$) (Fig. 8a). The third factor obtained with the 3-factor solution was identical to LV-OOA ($Q/Q_{exp} = 1.08$, $R = 0.98$).

The factor identification was confirmed by comparing the time series and mass spectra of each factor with external tracers (NO_3^-, SO_4^{2-}, NH_4^+, Cl^-, BC), available gas phase measurements (NO, NO_x, CO, SO_2 and O_3) and reference source mass spectra available on the AMS MS database
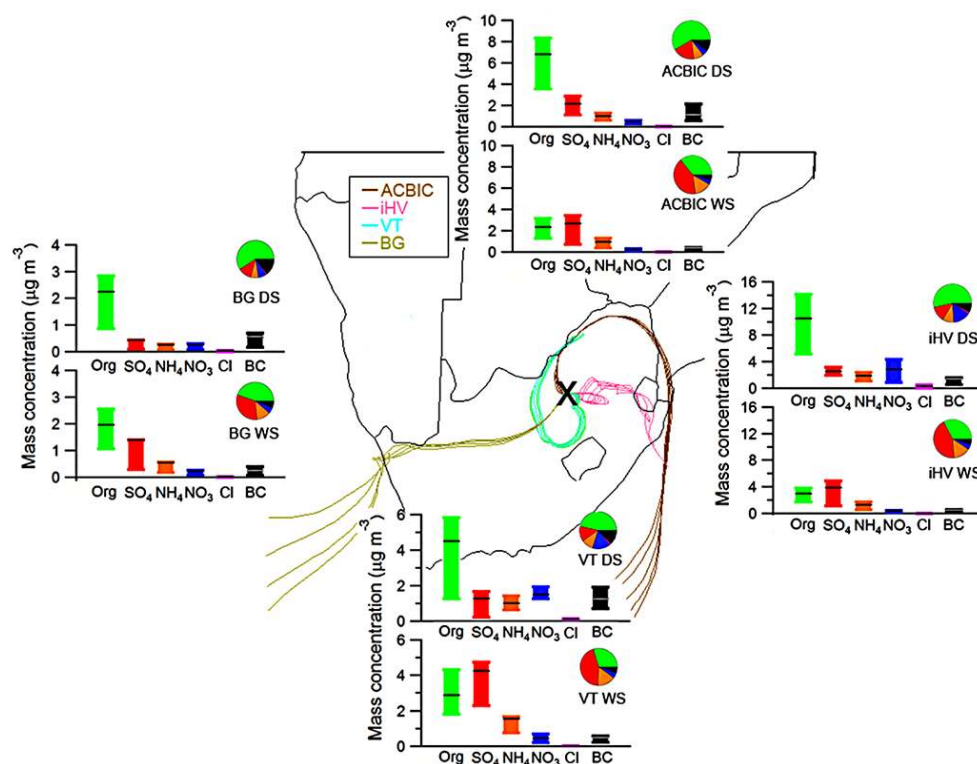
Fig. 7. Summary of NR-PM$_1$ + BC composition associated with each source region as well as representative 96 h backtrajectories marked in colours associated with the source regions. The box plots indicate 25th and 75th percentiles and the line within the box marks the mean. Location of the Welgegund measuring site is marked as a black cross.
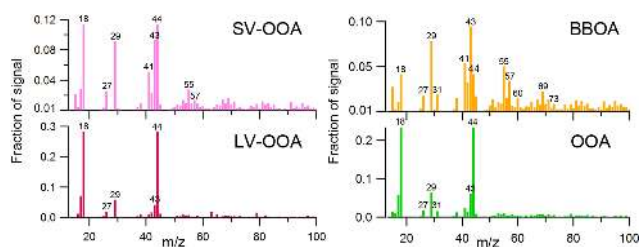

Fig. 8. OA mass spectra of **(a)** SV-OOA and LV-OOA (wet season) and **(b)** BBOA and OOA (dry season).

(Ulbrich, I. M., Lechner, M., and Jimenez, J. L., AMS Spectral Database, url: http://cires.colorado.edu/jimenez-group/AMSsd; Ulbrich et al., 2009). Solutions were further investigated for the "f peak" (Ulbrich et al., 2009) and seed influences on the mass spectra and time series. The factors obtained for different "f peak" values and the retained solutions were stable over the different starting points (seeds). Finally, the 2-factor solution rotated by "f peak" of 0.02 (dry season) appeared to represent our data the best. The factors were identified as OOA ($f_{43} = 6\%$, $f_{44} = 23\%$) and BBOA ($f_{60} = 1.5\%$, $f_{73} = 1\%$) (Fig. 8b), representing 4% and 33% of the total OA, respectively, with an unfitted fraction of 3%. The "f peak" value of 0.10 gave the best solution

for the wet season with LV-OOA ($f_{43} = 4\%$, $f_{44} = 28\%$) and SV-OOA ($f_{43} = 9\%$, $f_{44} = 11\%$) (Fig. 8a) representing 49% and 46% of the total OA, respectively, and an unfitted fraction of 6%.

The corresponding BBOA factor correlated with the standard BBOA published by Ng, et al. (2011b) ($R = 0.93$). The identified BBOA factor was also characterised by a contribution of the organic fragments m/z 60 and m/z 73, i.e., the levoglucosan marker fragments, which are considered to be tracers of biomass burning aerosols (Scheider et al., 2006; Alfarra et al., 2007; Lanz et al., 2008; Mohr et al., 2009). The BBOA factor correlated well with the combustion-related BC ($R = 0.81$), NO$_3^-$ ($R = 0.79$) and CO ($R = 0.72$) species. However, the best correlation of BBOA was found to be with Cl$^-$ ($R = 0.89$), although the observed Cl$^-$ concentrations were typically low. The correlation of the BBOA time series with BC, NO$_3^-$ and CO and the presence of the levoglucosan marker fragments in the BBOA and similar diurnal patterns profile verified its primary origin (see Figs. 4b and 9). The BBOA showed early morning and evening peaks (Fig. 9) and this type of a diurnal pattern could be reasonably attributed to the combined result of the low boundary layer height and burning events in the morning and evening.
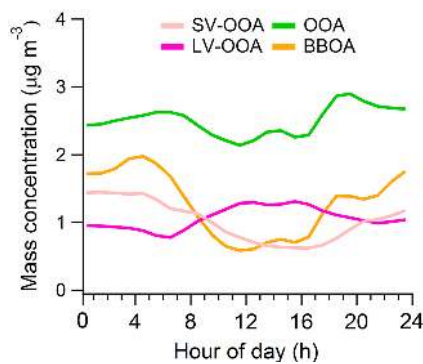
Fig. 9. Diurnal profiles of SV-OOA (WS), LV-OOA (WS), BBOA (DS) and OOA (DS).

The LV-OOA (wet season) and OOA (dry season) factors correlated well with the standard LV-OOA spectrum ($R > 0.95$, Ng et al., 2011b). The time series of these factors correlated with NH_4^+ ($R = 0.70$ and $R = 0.73$, respectively) and SO_4^{2-} ($R = 0.82$ and $R = 0.66$), and with the sum of SO_4^{2-} and NO_3^- ($R = 0.80$ and $R = 0.75$). Based on previous studies, low-volatile OOA can be explained in many cases by highly oxidized, aged, long-range-transported aerosol particles (e.g., Lanz et al., 2010; Raatikainen et al., 2010). It is important to note that the OA oxidation levels were high also when air masses passes over the iHV and VT (Fig. 10a), not only during aged, long-range-transported air masses. This indicates possible acid formation of LV-OOA (Liggio and Li, 2013). The significance of acidity will be discussed more detail in Sect. 3.5.2.

Higher daytime concentration of LV-OOA (Fig. 9) reflects its photochemical production in daytime. Moreover, the stronger vertical mixing in daytime may increase transport of aged organics from above the surface layer.

Contrary to what was found for the LV-OOA factor, the correlation of the OOA time series with the combustion tracers such as BC ($R = 0.62$) and CO ($R = 0.66$) supports the suggestions that part of the OOA is formed from combustion-related VOCs. The similarities in the diurnal patterns of OOA (Fig. 9) and SO_4^{2-} (Fig. 4b) support the secondary contribution of OOA (Zhang et al., 2011). Possible signs of the formation of SOA related to combustion emitted VOCs, peaking in the late afternoon, was observed in the OOA profile (Fig. 9).

The SV-OOA spectra correlated with the standard SV-OOA ($R = 0.83$, Ng, et al., 2011b). The time series of the SV-OOA correlated with NO_3^- ($R = 0.76$), a characteristic tracer for SV-OOA, but also with the combustion-related tracers BC ($R = 0.82$) and CO ($R = 0.72$). The diurnal cycle of SV-OOA (Fig. 9) was similar to that of both NO_3^- and Cl^- (Fig. 4a) which verifies its semi-volatile character. It results from the partitioning between the gaseous and particulate phase depending on the ambient temperature and humidity (e.g., Zhang et al., 2011).

The commonly-identified hydrocarbon organic aerosols (HOA) factor could not be isolated in this investigation, in line with studies by Hildebrandt et al. (2010) and Huang et al. (2011). HOA has been extensively identified in previous AMS measurements and is mainly attributed to primary combustion sources (Zhang et al., 2007a; Lanz et al., 2007, 2008; Ulbrich et al., 2009). In our case, HOA was probably mixed with the BBOA and SV-OOA factors. It is worth noting that most of the hydrocarbons were diluted by mixing of the surface mixing layer air and oxidized before arriving at the site.

3.5.2 Insight into OA properties and sources

It has been observed that f_{44} (m/z 44 divided by OA) correlate with the oxygen to carbon (O : C) ratio (Aiken et al., 2008) and the hygroscopicity of the SOA-dominated aerosols (Jimenez et al., 2009; Raatikainen et al., 2010). Therefore, f_{44} is an indicator of potential cloud condensation nuclei (CCN). Aiken et al. (2008) found a significant correlation between the O : C ratio and f_{44} described by the following least-squares fit:

$$O : C = (3.82 \pm 0.05) \cdot f_{44} + (0.079 \pm 0.0070),$$
$$\left[95\% \text{ CI, } R^2 = 0.84 \right] \tag{6}$$

Although this correlation was derived from the ambient measurements conducted in Mexico City, it provided an estimation of the O : C ratio of the average OA. Photochemical aging leads to an increase in f_{44} (Alfarra et al., 2004; Aiken et al., 2008), so the f_{44} axis in Fig. 10 is an indicator of atmospheric aging and the triangular space represent an area where OA compounds are usually found (Ng et al., 2010). Since f_{43} (m/z 43 divided by total OA) is indicative of less oxidized and photochemical younger organics than f_{44}, the variability in f_{43} arises from difference in OOA components because of different sources and chemical pathways (Ng et al., 2010). Figure 10b shows that, on average, OA measured at the Welgegund station was highly oxidized and more oxygenated in the wet season ($f_{44} = 19\%$, $f_{43} = 6\%$) than during the dry season ($f_{44} = 17\%$, $f_{43} = 7\%$). This dissimilarity between oxidation levels can be explained, in part, by the aerosol acidity as it has been shown that under acid seed aerosol conditions, oligomer formation associated with the uptake of organics is enhanced by a factor of three or more compared to neutral aerosols, with concomitant increase in the O : C ration (Liggio and Li, 2013). The average f_{44} corresponds to the O : C ratios of 0.8 and 0.7 (Eq. 6) during the wet and dry seasons, respectively. Statistical significance of the difference in O : C ratios were tested with the Wilcoxon rank sum test by using R-software (R Development Core Team, 2013). The difference between the seasons was found to be statistically significant ($p < 2.2 \times 10^{-16}$).

The properties of OA were further investigated by selecting representative daytime and nighttime air masses had passed over the four source regions. The iHV and VT plumes,
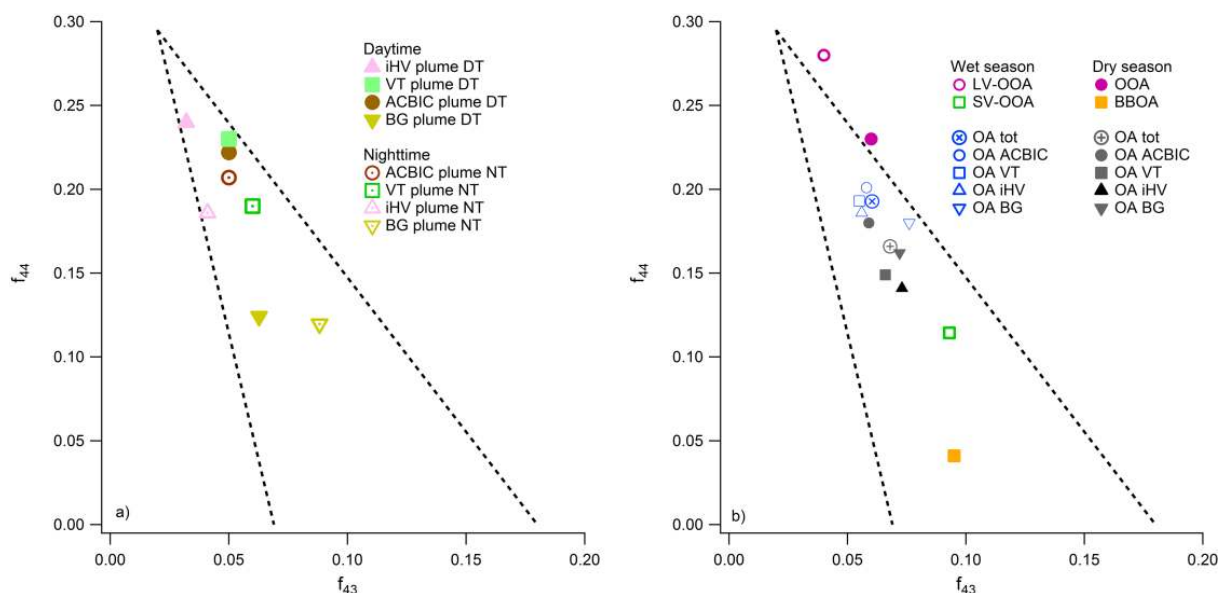
Fig. 10. Triangle plots **(a)** for day and nighttime source region plumes and **(b)** for source region averages and for indentified organic groups, i.e., LV-OOA, SV-OOA, OOA and BBOA. The dotted lines define the triangular space where ambient OA components usually fall. Triangle plot is described detail in Ng et al. (2010).

characterised by high SO$_4^{2-}$ concentrations, also had the highest daytime OA oxidation levels ($f_{44} = 24\%$ for iHV and $f_{44} = 23\%$ for VT) (Fig. 10a), which is consistent with oligomer formation in acidic conditions (Liggio and Li, 2013). The nighttime oxidation was significantly lower ($f_{44} = 19\%$) reflecting a lower level of solar radiation. In contrast to that, the BG air mass plume showed much lower OA oxidation ($f_{44} = 12\%$) levels (Fig. 10a), indicating a larger fraction of local sources like oxidation products of biogenic volatile organic compounds (BVOC) and local household combustion. Wood and low grade coal are the most common fuels used in household combustion for space heating and cooking in informal and semi-formal settlements (Venter et al., 2012). It should also be mentioned that the potential oxidant concentrations are significantly lower in the background area and the BG daytime and nighttime trajectories were not 100 % identical, which reflected by different f_{43} values.

As expected, both daytime and nighttime oxidation levels were high in the ACBIC plume (Fig. 10a) due to aerosol ageing during the anticyclonic circulation of air masses. Actually, the nighttime oxidation levels were higher in the ACBIC plume than in the iHV plume, which indicates that the intensity of solar radiation was less important in the ACBIC plume. The anticyclonic air flow on the northern Highveld in South Africa is the dominant flow pattern which increases the lifetime and ageing of atmospheric aerosols (Garstag et al., 1996; Tyson et al., 2000).

Finally, the mean oxidation levels for each region were calculated. These results showed that OA in the air masses that had passed over the ACBIC region was characterised

by highly oxidized organics in both the wet and dry seasons (Fig. 10b), whereas the other regions showed more variability between the seasons. In the dry season, the mean oxidation levels were the lowest in air masses that had passes over the iHV and VT regions, probably due to the large amounts of fresh combustion emissions, including savanna fires, traffic and household combustion, during the dry season. The lowest OA oxidation state in the wet season was observed for the BG region (Fig. 10b).

Overall, our results point out a high OA oxidization level in the Welgegund site; LV-OOA ($f_{43} = 4\%$, $f_{44} = 28\%$) and OOA ($f_{43} = 6\%$, $f_{44} = 23\%$). Oxidation levels were even higher than extent of OA oxidation of the FAME-08 and FAME-09 campaigns (Hildebrandt et al., 2010, 2011). Until now only the Okinawa measurement site have showed similar oxidation levels (Ng et al., 2010). In contrast to that, the oxidation level of SV-OOA ($f_{43} = 9\%$, $f_{44} = 11\%$) was at the same level as for sites in Northern Hemispheric datasets (Ng et al., 2010).

The source characterisation of BBOA, OOA, SV-OOA and LV-OOA for the four regions is presented in Fig. 11. The concentration of SV-OOA (Fig. 11a) showed only moderate differences between the different regions suggesting that major point sources do not have a large influence to SV-OOA factor. SV-OOA correlated with NO$_3^-$ in industrial regions and resembled to biogenic SV-OOA in Ng et al. (2010a). It is notable that the industrial regions in South Africa are located in the areas for which higher biogenic emissions are expected (e.g., grassland and savannah biomes) in the wet season, if compared to the BG (e.g., Kalahari and Karoo biomes). SV-OOA is factor from a variety of mixed sources
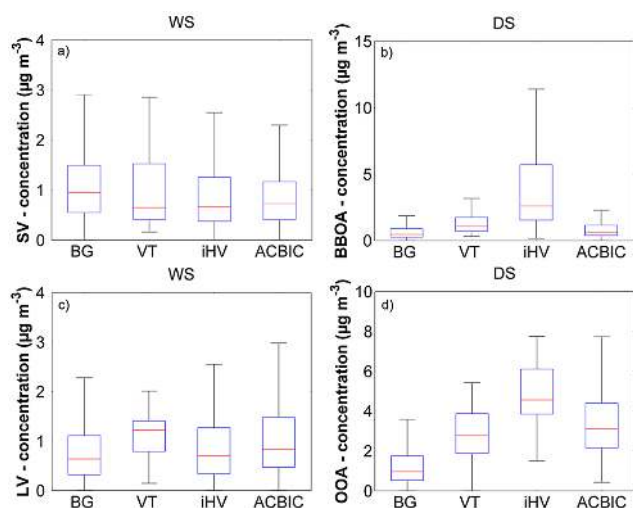
Fig. 11. Organic group characterisation for the four source regions, i.e., BG, VT, iHV and ACBIC, for both the wet season (WS) and the dry seasons (DS). The box plots indicate of 25th and 75th percentiles and the line within the box marks the median. Whiskers present 5th and 95th percentiles.

that are semi-volatile, so its diurnal trend was dominated by the temperature-dependent volatility behaviour, similar to NO$_3^-$.

In the dry season, the primary BBOA originated mainly from the iHV (Fig. 11b) region (more than 50 % of total BBOA), whereas a large fraction of the OOA (Fig. 11d) originated also from the VT and ACBIC regions. During the dry season the OA source regions (Fig. S1) appeared to follow the vegetation type so that the highest OA concentrations originate in the regions where vegetation has more biomass (e.g., Mucina and Rutherford, 2006). Addition to that incomplete combustion of coal and wood in ineffective appliances for household heating and cooking are common occurrences in the semi-formal and informal settlements (Venter et al., 2012). Therefore, the high quantity of domestic burning and cooking in the megacity region together with grassland fires enhance BBOA factor concentration in the iHV region.

The LV-OOA concentration was high when air masses passed VT region (Fig. 11c) similar to SO$_4^{2-}$ concentration (Fig. 6c) during wet season, which highlights the potential importance of aerosol acidity in OOA evolution. The maximum and 75–percentile concentrations of LV-OOA as well as the mean OA oxidation level in triangle plot (Fig. 10b) were high when air passed over ACBIC region which is consistent with long-range-transported aged aerosols (Fig. 11c).

4   Conclusions

This work presents the first long term NR-PM$_1$ chemical composition results for southern Africa, based on measurements conducted at the Welgegund measurements station in

the interior of South Africa. The NR-PM$_1$ mass concentrations varied largely from less than 1 μg m^{-3} to a maximum of 89 μg m^{-3}. The aerosol composition was dominated by OA and sulfates with the mean NR-PM$_1$ concentration of 7.5 μg m^{-3} and total PM$_1$ of 9.1 μg m^{-3}. Savanna fires occurring on a regional scale during the dry season increased both the primary combustion aerosols and the formation of secondary aerosols via combustion emitted precursor species.

A significant fraction of the NR-PM$_1$ aerosols consisted of OA (63 % of total OA in the dry season and 37 % in the wet season). The composition OA differed and its concentration levels varied considerably between the seasons due to different sources and atmospheric conditions. For example, BBOA represented 33 % of total OA in the dry season while no BBOA factor was identified in the wet season. In general, OA was highly oxidized with average O : C ratios of 0.8 and 0.7 during the wet and dry season, respectively. The high oxidation levels and the differences between the seasons could be explained, at least partially, by the acidity of the aerosols. Highly oxidized organic aerosols were observed both during iHV and VT plumes (characterised by high SO$_4^{2-}$ concentration) and anticyclone circulation (characterised by long range transported aged aerosols).

The results obtained from this investigation provide new insight on the seasonal differences in aerosol characteristics and associated sources, along with atmospheric processes connecting the sources with observed aerosol characteristics, in southern Africa. These features are quite different from those reported for more comprehensively-investigated aerosol systems in the Northern Hemisphere.

The results will directly assist policy makers in South Africa to implement the correct procedures to address current levels of atmospheric aerosols, as well as with their decision making for future industrial developments. Furthermore, the measurements conducted in this study signify the importance of these types of measurements in this region. The next step for aerosol research in this region would entail the implementation of long-term continuous chemical composition measurements with instruments such as the high resolution AMS.

Supplementary material related to this article is available online at http://www.atmos-chem-phys.net/14/1909/2014/acp-14-1909-2014-supplement.pdf.

References

Aiken, A. C., DeCarlo, P. F., and Jimenez, J. L.: Elemental analysis of organic species with electron ionization high-resolution mass spectrometry, Anal. Chem., 79, 8350–8358, doi:10.1021/ac071150w, 2007.

Aiken, A. C., DeCarlo, P. F., Kroll, J. H., Worsnop, D. R., Huffman, J. A., Docherty, K., Ulbrich, I. M., Mohr, C., Kimmel, J. R., Sueper, D., Sun, Y., Zhang, Q., Trimborn, A. M., Northway, M. J., Ziemann, P. J., Canagaratna, M. R., Alfarra, M. R., Prevot, A. S., Dommen, J., Duplissy, J., Metzger, A., Baltensperger, U., and Jimenez, J. L.: O/C and OM/OC ratios of primary, secondary, and ambient organic aerosols with High Resolution Time-of-Flight Aerosol Mass Spectrometry, Environ. Sci. Technol., 42, 4478–4485, 2008.

Air Resources Laboratory: Gridded Meteorological Data Archives, available at: http://www.arl.noaa.gov/archives.php (last access: 15 October 2012), 2012.

Akagi, S. K., Craven, J. S., Taylor, J. W., McMeeking, G. R., Yokelson, R. J., Burling, I. R., Urbanski, S. P., Wold, C. E., Seinfeld, J. H., Coe, H., Alvarado, M. J., and Weise, D. R.: Evolution of trace gases and particles emitted by a chaparral fire in California, Atmos. Chem. Phys., 12, 1397–1421, doi:10.5194/acp-12-1397-2012, 2012.

Alfarra, M. R., Coe, H., Allan, J. D., Bower, K. N., Boudries, H., Canagaratna, M. R., Jimenez, J. L., Jayne, J. T., Garforth, A., Li, S. M., and Worsnop, D. R.: Characterisation of urban and rural organic aerosols in the lower Fraser Valley using two Aerodyne particulate mass spectrometers, Atmos. Environ., 38, 5745–5758, 2004.

Alfarra, M. R., Prevot, A., Szidat, S., Sandradewi, J., Weimer, S., Lanz, V., Scheiber, D., Mohr, M., and Baltensperger, U.: Identification of the mass spectral signature of organic aerosols from wood burning emissions, Environ. Sci. Technol., 41, 5770–5777, 2007.

Allan, J., Jimenez, J., Williams, P., Alfarra, M., Bower, K., Jayne, J., Coe, H., and Worsnop, D.: Quantitative sampling using an Aerodyne aerosol mass spectrometer 1. techniques of data interpretation and error analysis, J. Geophys. Res., 108, 4090, doi:10.1029/2002JD002358, 2003.

Allan, J., Delia, A. E., Coe, H., Bower, K. N., Alfrrara, R., Jimenez, J. L., Middlebrook, A. M., Drewnick, F., Onasch, T. B., Canagaratna, M. R., Jayne, J., and Worsnop, D. R.: Technical note: a generalised method for the extraction of chemically resolved mass spectra from Aerodyne aerosol mass spectrometer data, J. Aerosol Sci., 35, 909–922, 2004.

Beukes, P., Dawson, N., and van Zyl, P. G.: Theoretical and practical aspect of Cr (VI) in the South African FeCr industry, S. African Inst. Min. M., 110, 743–750, 2010.

Beukes, P., Vakkari, V., van Zyl, P. G., Venter, A., Josipovic, M., Jaars, K., Tiitta, P., Laakso, H., Kulmala, M., Worsnop, D., Pienaar, J., Järvinen, E., Chellapermal, R., Ignatius, K., Maalisck, Z., Cesnulyte, V., Ripamonti, G., Laban T., Skrabalova, L., du Toit, M., Virkkula, A., and Laakso L.: Source region plume characterisation of the interior of South Africa, as measured at Welgegund, Atmos. Chem. Phys., in preparation, 2014.

Boko, M. I., Niang, A., Nyong, C., Vogel, A., Githeko, M., Medany, B., Osman-Elasha, R., Tabo, and Yanda, P.: Africa, in. Climate Change 2007: impacts, adaptation and vulnerability. contribution of working group II to the fourth assessment report of the intergovernmental panel on climate change, edited by: Parry, M. L., Canziani, O. F., Palutikof, J. P., van der Linden, P. J., and Hanson, C. E., Cambridge University Press, Cambridge UK, 433–467, 2007.

Brunke, E.-G., Labuschagne, C., Ebinghaus, R., Kock, H. H., and Slemr, F.: Gaseous elemental mercury depletion events observed at Cape Point during 2007–2008, Atmos. Chem. Phys., 10, 1121–1131, doi:10.5194/acp-10-1121-2010, 2010.

Canagaratna, M., Jayne, J., Jimenez, J., Allan, J., Alfarra, M., Zhang, Q., Onasch, T., Drewnick, F., Coe, H., Middlebrook, A., Delia, A., Williams, L., Trimborn, A., Northway, M., DeCarlo, P., Kolb, C., Davidovits, P., and Worsnop, D.: Chemical and microphysical characterisation of ambient aerosols with the Aerodyne aerosol mass spectrometer, Mass Spectrom. Rev., 26, 185–222, 2007.

Clegg, S. L., Brimblecombe, P., and Wexler, A. S.: Thermodynamical model of the system H-NH$_4^+$-SO$_4^{2-}$-NO$_3^-$-H$_2$O at tropospheric temperatures, J. Phys. Chem. A, 102, 2137–2154, 1998.

Cramer, L., Basson, J., and Nelson, L.: The impact of platinum production from UG2 ore on ferrochrome production in South Africa, S. African Inst. Min. M., 104, 517–527, 2004.

Draxler, R. R. and Hess, G. D.: Description of the HYSPLIT 4 Modelling System, NOAA Technical Memorandum ERL ARL–224, 2004.

DeCarlo, P., Kimmel, J., Trimborn, A., Northway, M., Jayne, J., Aiken, A., Gonin, M., Fuhrer, K., Horvart, T., Docherty, K., Worsnop, D., and Jimenez J.: A field-deployable high-resolution time-of-flight aerosol mass spectrometer, Anal. Chem., 78, 8281–8289, 2006.

Fishman, J. J., Hoell Jr., R. D., Bendura, R. J., McNeal, V. W., and Kirchhoff, J. H.: NASA GTE TRACE-A Experiment (September–October 1992), overview, J. Geophys. Res., 101, 23865–23880, 1996.

Eatough, D. J., Eatough, N. L., Pang, Y., Sizemore, S., Kirchstetter, T. W., Novakov, T., and Hobbs, P. V.: Semi-volatile particulate organic material in southern Africa during SAFARI-2000, J. Geophys. Res., 108, 8479, doi:10.1029/2002JD002296, 2003.

Forster, P. V., Ramaswamy, P., Artaxo, T., Berntsen, R., Betts, D. W., Fahey, J., Haywood, J., Lean, D. C., Lowe, G., Myhre, J., Nganga, R., Prinn, G., Raga, M., Schultz, M., and Van Dorland, R.: Changes in atmospheric constituents and in radiative forcing, in: Climate Change 2007: The Physical Science Basis, contribution of Working Group I to the Fourth Assessment Report of the Intergovernmental Panel on Climate Change, edited by: Solomon, S., Qin, D., Manning, M., Chen, Z., Marquis, M., Averyt, K. B., Tignor, M., and Miller, H. L., Cambridge University Press, Cambridge, UK and New York, NY, USA, 129–234, 2007.

Garstang, M., Tyson, P. D., Swap, R., Edwards, M., Kållberg, P., and Lindesay, J. A.: Horizontal and vertical transport of air over southern Africa, J. Geophys. Res., 101, 23721–23736, 1996.

Hildebrandt, L., Engelhart, G. J., Mohr, C., Kostenidou, E., Lanz, V. A., Bougiatioti, A., DeCarlo, P. F., Prevot, A. S. H., Baltensperger, U., Mihalopoulos, N., Donahue, N. M., and Pandis, S. N.: Aged organic aerosol in the Eastern Mediterranean: the Finokalia Aerosol Measurement Experiment – 2008, Atmos. Chem. Phys., 10, 4167–4186, doi:10.5194/acp-10-4167-2010, 2010.

Hildebrandt, L., Kostenidou, E., Mihalopoulos, N., Worsnop, D. R., Donahue, N. M., and Pandis, S. N.: Formation of highly

oxygenated organic aerosol in the atmosphere: insights from the Finokalia Aerosol Measurement Experiments, Geophys. Res. Lett., 37, L23801, doi:10.1029/2010GL045193, 2011.

Hirsikko, A., Vakkari, V., Tiitta, P., Manninen, H. E., Gagné, S., Laakso, H., Kulmala, M., Mirme, A., Mirme, S., Mabaso, D., Beukes, J. P., and Laakso, L.: Characterisation of sub-micron particle number concentrations and formation events in the western Bushveld Igneous Complex, South Africa, Atmos. Chem. Phys., 12, 3951–3967, doi:10.5194/acp-12-3951-2012, 2012.

Hirsikko, A., Vakkari, V., Tiitta, P., Hatakka, J., Kerminen, V.-M., Sundström, A.-M., Beukes, J. P., Manninen, H. E., Kulmala, M., and Laakso, L.: Multiple daytime nucleation events in semi-clean savannah and industrial environments in South Africa: analysis based on observations, Atmos. Chem. Phys., 13, 5523–5532, doi:10.5194/acp-13-5523-2013, 2013.

Hobbs, P. V.: Clean air slots amid dense atmospheric pollution in Southern Africa, J. Geophys. Res., 108, 8490, doi:10.1029/2002JD002156, 2003.

Huang, X.-F., He, L.-Y., Hu, M., Canagaratna, M. R., Kroll, J. H., Ng, N. L., Zhang, Y.-H., Lin, Y., Xue, L., Sun, T.-L., Liu, X.-G., Shao, M., Jayne, J. T., and Worsnop, D. R.: Characterisation of submicron aerosols at a rural site in Pearl River Delta of China using an Aerodyne High-Resolution Aerosol Mass Spectrometer, Atmos. Chem. Phys., 11, 1865–1877, doi:10.5194/acp-11-1865-2011, 2011.

Huffman, J. A., Jayne, J. T., Drewnick, F., Aiken, A. C., Onasch, T., Worsnop, D. R., and Jimenez, J. L.: Design, modeling, optimization, and experimental tests of a particle beam width probe for the Aerodyne aerosol mass spectrometer, Aerosol Sci. Tech., 39, 1143–1163, doi:10.1080/02786820500423782, 2005.

Jang, M. S., Czoschke, N. M., Lee, S., and Kamens, R. M.: Heterogeneous atmospheric aerosol production by acid-catalyzed particle-phase reactions, Science, 298, 814–817, 2002.

Jayne, J., Leard, D., Zhang, X., Davidovits, P., Smith, K., Kolb, C., and Worsnop, D.: Development of an aerosol mass spectrometer for size and composition analysis of submicron particles, Aerosol Sci. Tech., 33, 49–70, 2000.

Jimenez, J. L., Jayne, J. T., Shi, Q., Kolb, C. E., Worsnop, D. R., Yourshaw, I., Seinfeld, J. H., Flagan, R. C., Zhang, X., Smith, K. A., Morris, J., and Davidovits, P.: Ambient aerosol sampling with an aerosol mass spectrometer. J. Geophys. Res.-Atmos., 108, 8425, doi:10.1029/2001JD001213, 2003.

Jimenez, J. L., Canagaratna, M. R., Donahue, N. M., Prevot, A. S., Zhang, Q., Kroll, J. H., DeCarlo, P. F., Allan, J. D., Coe, H., Ng, N. L., Aiken, A. C., Docherty, K. D., Ulbrich, I. M., Grieshop, A. P., Robinson, A. L., Duplissy, J., Smith, J. D., Wilson, K .R., Lanz, V. A., Hueglin, C., Sun, Y. L., Tian, J., Laaksonen, A., Raatikainen, T., Rautiainen, J., Vaattovaara, P., Ehn, M., Kulmala, M., Tomlinson, J. M., Collins, D. R., Cubison , M. J., Dunlea, E. J., Huffman, J. A., Onasch, T. B., Alfarra, M. R., Williams, P. I., Bower, K., Kondo, Y., Schneider, J., Drewnick, F., Borrmann, S., Weimer, S., Demerjian, K., Salcedo, D., Cottrell, L., Griffin, R., Takami, A., Miyoshi, T., Hatakeyama, S., Shimono, A., Sun, J. Y., Zhang, Y. M., Dzepina, K., Kimmel, J. R., Sueper, D., Jayne, J. T., Herndon, S. C., Trimborn, A. M. Williams, L. R., Wood, E. C., Kolb, C. E., Middlebrook, A. M., Baltensperger, U., and Worsnop, D. R.: Evolution of organic aerosols in the atmosphere, Science, 326, 1525–1529, doi:10.1126/science.1180353, 2009.

Josipovic, M., Annegarn H., Kneen, M., Pienaar, J., and Piketh, S.: Concentrations, distributions and critical level exceedance assessment of SO$_2$, NO$_2$ and O$_3$ in South Africa, Environ. Monit. Assess., 171, 181–196, 2010.

Kanakidou, M., Seinfeld, J. H., Pandis, S. N., Barnes, I., Dentener, F. J., Facchini, M. C., Van Dingenen, R., Ervens, B., Nenes, A., Nielsen, C. J., Swietlicki, E., Putaud, J. P., Balkanski, Y., Fuzzi, S., Horth, J., Moortgat, G. K., Winterhalter, R., Myhre, C. E. L., Tsigaridis, K., Vignati, E., Stephanou, E. G., and Wilson, J.: Organic aerosol and global climate modelling: a review, Atmos. Chem. Phys., 5, 1053–1123, doi:10.5194/acp-5-1053-2005, 2005.

Kirchstetter, T. W., Novakov, T., Hobbs, P. W., and Magi, B.: Airborne measurements of carbonaceous aerosols in southern Africa during the dry biomass burning season, J. Geophys. Res, 108, 8476, doi:10.1029/2002JD002171, 2003.

Laakso, L., Laakso, H., Aalto, P. P., Keronen, P., Petäjä, T., Nieminen, T., Pohja, T., Siivola, E., Kulmala, M., Kgabi, N., Molefe, M., Mabaso, D., Phalatse, D., Pienaar, K., and Kerminen, V.-M.: Basic characteristics of atmospheric particles, trace gases and meteorology in a relatively clean Southern African Savannah environment, Atmos. Chem. Phys., 8, 4823–4839, doi:10.5194/acp-8-4823-2008, 2008.

Laakso, L., Vakkari, V., Virkkula, A., Laakso, H., Backman, J., Kulmala, M., Beukes, J. P., van Zyl, P. G., Tiitta, P., Josipovic, M., Pienaar, J. J., Chiloane, K., Gilardoni, S., Vignati, E., Wiedensohler, A., Tuch, T., Birmili, W., Piketh, S., Collett, K., Fourie, G. D., Komppula, M., Lihavainen, H., de Leeuw, G., and Kerminen, V.-M.: South African EUCAARI measurements: seasonal variation of trace gases and aerosol optical properties, Atmos. Chem. Phys., 12, 1847–1864, doi:10.5194/acp-12-1847-2012, 2012.

Laakso, L., Merikanto, J., Vakkari, V., Laakso, H., Kulmala, M., Molefe, M., Kgabi, N., Mabaso, D., Carslaw, K. S., Spracklen, D. V., Lee, L. A., Reddington, C. L., and Kerminen, V.-M.: Boundary layer nucleation as a source of new CCN in savannah environment, Atmos. Chem. Phys., 13, 1957–1972, doi:10.5194/acp-13-1957-2013, 2013.

Lanz, V. A., Alfarra, M. R., Baltensperger, U., Buchmann, B., Hueglin, C., and Prévôt, A. S. H.: Source apportionment of submicron organic aerosols at an urban site by factor analytical modelling of aerosol mass spectra, Atmos. Chem. Phys., 7, 1503–1522, doi:10.5194/acp-7-1503-2007, 2007.

Lanz, V. A., Alfarra, M., Baltensperger, U., Buchmann, B., Hueglin, C., Szidat, S., Wehrli, M., Wacker, L., Weimer, S., Caseiro, A., Puxbaum, H., and Prévôt, A.: Source attribution of submicron organic aerosols during wintertime inversions by advanced factor analysis of aerosol mass spectra, Environ. Sci. Technol., 42, 214–220, doi:10.1021/es0707207, 2008.

Lanz, V. A., Prévôt, A. S. H., Alfarra, M. R., Weimer, S., Mohr, C., DeCarlo, P. F., Gianini, M. F. D., Hueglin, C., Schneider, J., Favez, O., D'Anna, B., George, C., and Baltensperger, U.: Characterisation of aerosol chemical composition with aerosol mass spectrometry in Central Europe: an overview, Atmos. Chem. Phys., 10, 10453–10471, doi:10.5194/acp-10-10453-2010, 2010.

Liang, J. and Jacobson, M. Z.: A study of sulfur dioxide oxidation pathways over a range of liquid water contents, pH values, and temperatures, J. Geophys. Res., 104, 13749–13769, doi:10.1029/1999JD900097, 1999.

Liggio, J. and Li, S.-M.: A new source of oxygenated organic aerosol and oligomers, Atmos. Chem. Phys., 13, 2989–3002, doi:10.5194/acp-13-2989-2013, 2013.

Lindesay, J. A., Andreae, M. O., Goldammer, J. G., Harris, G., Annegarn, H. J,. Garstang, M., Scholes, R. J., and van Wilgen, B. W.: International geosphere-biosphere programme/international global atmospheric chemistry, SAFARI 92 field experiment: background and overview, J. Geophys. Res, 101, 23521–23530, doi:10.1029/96JD01512, 1996.

Liu, P., Ziemann, P., Kittelson, D., and McMurry, P.: Generating particle beams of controlled dimensions and divergence. 2. Experimental evaluation of particle motion in aerodynamic lenses and nozzle expansions, Aerosol Sci. Tech., 22, 314–324, 1995.

Liu, P. S. K., Deng, R., Smith, K. A., Williams, L. R., Jayne, J. T., Canagaratna, M. R., Moore, K., Onasch, T. B., Worsnop, D. R., and Deshler, T.: Transmission efficiency of an aerodynamic focusing lens system: comparison of model calculations and laboratory measurements for the Aerodyne Aerosol Mass Spectrometer, Aerosol. Sci. Tech., 41, 721–733, 2007.

Lourens, A. S., Beukes, J. P., van Zyl, P. G., Fourie, G., Burger, J., Pienaar, J. J., Read, C., and Jordan, J.: Spatial and temporal assessment of gaseous pollutants in the Highveld of South Africa, S. Afr. J. Sci., 107, 269, doi:10.4102/sajs.v107i1/2.269, 2011.

Lourens, A. S., Butler, T., Beukes J., van Zyl, P. G., Steffen, B., Wagner, T., Heue, K.-P., Pienaar, J. J., Fourier, G., and Lawrence, M.: Re-evaluating the NO₂ hotspot over the South African Highveld, S. Afr. J. Sci., 108, 1146, doi:10.4102/sajs.v108i11/12.1146, 2012.

Martin, S. T., Schlenker, J. C., Malinowski, A., Hung, H.-M., and Rudich, Y.: Crystallization of atmospheric sulfate-nitrate-ammonium particles, Geophys. Res. Lett., 30, 2102, doi:10.1029/2003GL017930, 2003.

Martins, J., Dhammapala, R., Lauchmann, G., Galy-Lacaux, C., and Pienaar, J.: Long-term measurements of sulphur dioxide, nitrogen dioxide, ammonia, nitric acid and ozone in southern Africa using passive samplers, S. Afr. J. Sci., 103, 336–342, 2007.

Matthew, B., Middlebrook, A., and Onasch, T.: Collection efficiencies in an Aerodyne aerosol mass spectrometer as a function of particle phase for laboratory generated aerosols, Aerosol Sci. Tech., 42, 884–898, 2008.

Mertes, S., Schröder, F., and Wiedensohler, A.: The particle detection efficiency curve of the TSI-3010 CPC as a function of temperature difference between saturator and condenser, Aerosol Sci. Tech., 23, 257–261, 1995.

Mensah, A. A., Holzinger, R., Otjes, R., Trimborn, A., Mentel, Th. F., ten Brink, H., Henzing, B., and Kiendler-Scharr, A.: Aerosol chemical composition at Cabauw, The Netherlands as observed in two intensive periods in May 2008 and March 2009, Atmos. Chem. Phys., 12, 4723–4742, doi:10.5194/acp-12-4723-2012, 2012.

Middlebrook, A. M., Bahreini, R., Jimenez, J. L., and Canagaratna, M.: Evaluation of composition dependent collection efficiencies for the Aerodyne aerosol mass spectrometer using field data, Aerosol Sci. Tech. 46, 258–271, doi:10.1080/02786826.2011.620041, 2012.

Mohr, C., Huffman, A., Cubison, M., Aiken, A., Docherty, K., Kimmel, J., Ulbricht, I., Hannigan, M., and Jimenez, J.: Characterisation of primary organic aerosol emissions from meat cooking, trash burning, and motor vehicles with high-resolution aerosol

mass spectrometry and comparison with ambient and chamber observations, Environ. Sci. Technol., 43, 2443–2449, 2009.

Moffet, R., Desyaterik, Y., Hopkins, R., Tivanski, A., Gilles, M., Wang, Y., Shutthanandan, V., Molina, L., Abraham, R., Johnson, K., Mugica, V., Molina, M., Laskin, A., and Prather, K.: Characterisation of aerosols containing Zn, Pb and Cl from an industrial region of Mexico city, Environ. Sci. Technol., 42, 7091–7097, 2008.

Mucina, L. and Rutherford, M. C. (Eds.): The vegetation of South Africa, Lesotho and Swaziland, South African National Biodiversity Institute, Pretoria, Republic of South Africa, 2006.

Ng, N. L., Canagaratna, M. R., Zhang, Q., Jimenez, J. L., Tian, J., Ulbrich, I. M., Kroll, J. H., Docherty, K. S., Chhabra, P. S., Bahreini, R., Murphy, S. M., Seinfeld, J. H., Hildebrandt, L., Donahue, N. M., DeCarlo, P. F., Lanz, V. A., Prévôt, A. S. H., Dinar, E., Rudich, Y., and Worsnop, D. R.: Organic aerosol components observed in Northern Hemispheric datasets from Aerosol Mass Spectrometry, Atmos. Chem. Phys., 10, 4625–4641, doi:10.5194/acp-10-4625-2010, 2010.

Ng, N., Herndon, S., Trimborn, A., Canagaratna, M., Croteau, P., Onasch, T., Suaper, D., Worsnop, D., Zhang, Q., and Sun, Y.: An Aerosol Chemical Speciation Monitor (ACSM) for routine monitoring of the composition and mass concentrations of ambient aerosol, Aerosol Sci. Tech., 45, 780–794, 2011a.

Ng, N., Canagaratna, M., Jimenez, J., Zhang, Q., Ulbricht, I., and Worsnop, D.: Real-time methods for estimating organics component mass concentrations from Aerosol Mass Spectrometry data, Environ. Sci. Technol., 45, 910–916, 2011b.

Paatero, P.: Least squares formulation of robust non-negative factor analysis, Chemometr. Intell. Lab., 37, 23–35, 1997.

Paatero, P. and Tapper, U.: Positive matrix factorization: a non-negative factor model with optimal utilisation of error estimates of data values, Environmetrics, 5, 111–126, doi:10.1002/env.3170050203, 1994.

Pathak, R. K., Wang, T., Ho, K. F., and Lee, S. C.: Characteristics of summertime PM₂.₅ organic and elemental carbon in four major Chinese cities: implications of high acidity for water-soluble organic carbon (WSOC), Atmos. Environ., 45, 318–325, 2011.

Petäjä, T., Vakkari, V., Pohja, T., Nieminen, T., Laakso, H., Aalto, P. P., Keronen, P., Siivola, E., Kerminen, V.-M., Kulmala, M., and Laakso, L.: Transportable aerosol characterisation trailer with trace gas chemistry: design, instruments and verification, Aerosol Air Qual. Res., 13, 421–435, 2013.

R Development Core Team: R: A language and environment for statistical computing, R Foundation for Statistical Computing, Vienna, 2013.

Raatikainen, T., Vaattovaara, P., Tiitta, P., Miettinen, P., Rautiainen, J., Ehn, M., Kulmala, M., Laaksonen, A., and Worsnop, D. R.: Physicochemical properties and origin of organic groups detected in boreal forest using an aerosol mass spectrometer, Atmos. Chem. Phys., 10, 2063–2077, doi:10.5194/acp-10-2063-2010, 2010.

Riddle, E. E., Voss, P. B., Stohl, A., Holcomb, D., Maczka, D., Washburn, K., and Talbot, R. W.: Trajectory model validation using newly developed altitude-controlled balloons during the International Consortium for Atmospheric Research on Transport and Transformations 2004 campaign, J. Geophys. Res., 111, D23S57, doi:10.1029/2006JD007456, 2006.

Ross, K. E., Piketh, S. J., Bruintjes, R. T., Burger, R. P., Swap, R. J., and Annegarn, H. J.: Spatial and seasonal variations in CCN distributions and the aerosol-CCN relationship over southern Africa, J. Geophys. Res., 108, 8481, doi:10.1029/2002JD002384, 2003.

Salcedo, D., Onasch, T. B., Dzepina, K., Canagaratna, M. R., Zhang, Q., Huffman, J. A., DeCarlo, P. F., Jayne, J. T., Mortimer, P., Worsnop, D. R., Kolb, C. E., Johnson, K. S., Zuberi, B., Marr, L. C., Volkamer, R., Molina, L. T., Molina, M. J., Cardenas, B., Bernabé, R. M., Márquez, C., Gaffney, J. S., Marley, N. A., Laskin, A., Shutthanandan, V., Xie, Y., Brune, W., Lesher, R., Shirley, T., and Jimenez, J. L.: Characterisation of ambient aerosols in Mexico City during the MCMA-2003 campaign with Aerosol Mass Spectrometry: results from the CENICA Supersite, Atmos. Chem. Phys., 6, 925–946, doi:10.5194/acp-6-925-2006, 2006.

Seinfeld, J. H. and Pandis S. N.: Atmospheric Chemistry and Physics: from Air Pollution to Climate Change, 2nd Edn., J. Wiley & Sons, New York, 2006.

Shen, X., Lee, T., Guo, J., Wang, X., Li, P., Xu, P., Wang, Y., Ren, Y., Wang, W., Wang, T., Li, Y., Carn, S. A., and Collett Jr., J. L.: Aqueous phase sulfate production in clouds in eastern China, Atmos. Environ., 62, 502–511, 2012.

Siversten, B., Matal, C., and Rereira, L. M.: Sulphur emissions and transfrontier air pollution in southern Africa, Report 35, SADC ELMS, Lesotho, 117 pp., 1995.

Scheider, J., Weimer, S., Drewnick, F., Borrmann, S., Helas, G., Gwaze, P., Schmid, O., Andreae, M. O., and Kirchner, U.: Mass spectrometry analysis and aerodynamic properties of various types of combustion-related aerosol particles, Int. J. Mass. Spectrom. 258, 37–49, 2006.

Sun, J., Zhang, Q., Canagaratna, M. R., Zhang, Y., Ng, N. L., Sun, Y., Jayne, J. T., Zhang, X., and Worsnop, D. R.: Highly time- and size-resolved characterisation of submicron aerosol particles in Beijing using an Aerodyne Aerosol Mass Spectrometer, Atmos. Environ., 44, 131–140, 2010.

Sun, Y.-L., Zhang, Q., Schwab, J. J., Demerjian, K. L., Chen, W.-N., Bae, M.-S., Hung, H.-M., Hogrefe, O., Frank, B., Rattigan, O. V., and Lin, Y.-C.: Characterisation of the sources and processes of organic and inorganic aerosols in New York city with a high-resolution time-of-flight aerosol mass apectrometer, Atmos. Chem. Phys., 11, 1581–1602, doi:10.5194/acp-11-1581-2011, 2011.

Stohl, A.: Computation, accuracy and application of trajectories – a review and bibliography, Atmos. Environ., 32, 947–966, 1998.

Swap, R. J., Annegarn, H. J., Suttles, J. T., King, M. D., Platnick, S., Privette, J. L., and Scholes, R. J.: Africa burning: a thematic analysis of the Southern African Regional Science Initiative (SAFARI 2000), J. Geophys. Res., 108, 8465, doi:10.1029/2003JD003747, 2003.

Tyson, P. D. and Preston-Whyte, R. A.: The weather and climate of southern Africa, Oxford University press, Oxford, UK, 2000.

Ulbrich, I. M., Canagaratna, M. R., Zhang, Q., Worsnop, D. R., and Jimenez, J. L.: Interpretation of organic components from Positive Matrix Factorization of aerosol mass spectrometric data, Atmos. Chem. Phys., 9, 2891–2918, doi:10.5194/acp-9-2891-2009, 2009.

Vakkari, V., Laakso, H., Kulmala, M., Laaksonen, A., Mabaso, D., Molefe, M., Kgabi, N., and Laakso, L.: New particle forma-tion events in semi-clean South African savannah, Atmos. Chem. Phys., 11, 3333–3346, doi:10.5194/acp-11-3333-2011, 2011.

Vakkari, V., Beukes, J. P., Laakso, H., Mabaso, D., Pienaar, J. J., Kulmala, M., and Laakso, L.: Long-term observations of aerosol size distributions in semi-clean and polluted savannah in South Africa, Atmos. Chem. Phys., 13, 1751–1770, doi:10.5194/acp-13-1751-2013, 2013.

Vakkari, V., Kerminen, V.-M., Beukes, J. P., Tiitta, P., van Zyl, P. G., Josipovic, M., Venter, A. D., Jaars, K., Kulmala, M., and Laakso, L.: Rapid changes in biomass burning aerosols by atmospheric oxidation, in preparation, 2014.

Venter, A. D., Vakkari, V., Beukes, J. P., van Zyl, P. G., Laakso, H., Mabaso, D., Tiitta, P., Josipovic, M., Kulmala, M., Pienaar, J. J., and Laakso, L.: An air quality assessment in the industrialised western Bushveld Ignous Complex, South Africa, S. Afr. J. Sci., 108, 1059, doi:104102/sajs.v108i9/10.1059, 2012.

Wiedensohler, A.: An approximation of the bipolar charge-distribution for particles in the sub-micron size range, J. Aerosol Sci., 19, 387–389, 1998.

Winklmayr, W., Reischl, G., Lindnet, A., and Berner, A.: A new electromobility spectrometer for the measurement of aerosol size distribution in the size range from 1 to 1000 nm, J. Aerosol Sci., 22, 289–296, 1991.

Zhang, H., Wang, S., Hao, J., Wan, L., Jiang, J., Zhang, M., Mestl, H. E. S., Alnes, L. W. H., Aunan, K., and Mellouki, A. W.: Chemical and size characterisation of particles emitted from 30 the burning of coal and wood in rural households in Guizhou, China, Atmos. Environ., 51, 94–99, doi:10.1016/j.atmosenv.2012.01.042, 2012.

Zhang, Q., Alfarra, M. R., Worsnop, D. R., Allan, J. D., Coe, H., Canagaratna, M. R., and Jimenez, J. L.: Deconvolution and quantification of hydrocarbon-like and oxygenated organic aerosols based on aerosol mass spectrometry, Environ. Sci. Technol., 39, 4938–4952, doi:10.1021/es048568L, 2005a.

Zhang, Q., Canagaratna, M. R., Jayne, J. T., Worsnop, D. R., and Jimenez, J.-L.: Time- and size-resolved chemical composition of submicron particles in Pittsburgh: implications for aerosol sources and processes, J. Geophys. Res., 110, D07S09, doi:10.1029/2004JD004649, 2005b.

Zhang, Q., Jimenez, J. L., Canagaratna, M. R., Allan, J. D., Coe, H., Ulbrich, I., Alfarra, M. R., Takami, A., Middlebrook, A. M., Sun, Y. L., Dzepina, K., Dunlea, E., Docherty, K., DeCarlo, P. F., Salcedo, D., Onasch, T., Jayne, J. T., Miyoshi, T., Shimono, A., Hatakeyama, S., Takegawa, N., Kondo, Y., Schneider, J., Drewnick, F., Borrmann, S., Weimer, S., Demerjian, K., Williams, P., Bower, K., Bahreini, R., Cottrell, L., Griffin, R. J., Rautiainen, J., Sun, J. Y., Zhang, Y. M., and Worsnop, D. R.: Ubiquity and dominance of oxygenated species in organic aerosols in anthropogenically-influenced Northern Hemisphere mid-latitudes, Geophys. Res. Lett., 34, L13801, doi:10.1029/2007GL029979, 2007a.

Zhang, Q., Jimenez, J. L., Worsnop, D. R., and Canagaratna, M.: A case study of urban particle acidity and its influence on secondary organic aerosol, Environ. Sci. Technol., 41, 3213–3219, 2007b.

Zhang, Q., Jimenez, J.-L., Canagaratna, M. R., Ulbrich, I. M., Nga, L. N., Worsnop, D. R., and Sun, Y.: Understanding atmospheric organic aerosol via factor analysis of aerosol mass spectrometry: a review, Anal. Bioanal. Chem., 401, 3045–3067, doi:10.1007/s00216-011-5355-y, 2011.

Zunckel, M., Venjonoka, K., Pienaar, J. J., Brunke, E.-G., Pretorius, O., Koosialee, A., Raghunandan, A., and van Tienhoven, A. M: Surface ozone over southern Africa: synthesis of monitoring results during the Cross border Air Pollution Impact Assessment project, Atmos. Environ., 38, 6139–6147, 2004.